Boosted Dark Matter from Primordial Black Holes produced in a First-Order Phase Transition

Po-Yan Tseng (*National Tsing Hua U., TW*)
Danny Marfatia (*U. of Hawaii, Manoa, US*)

References:
JHEP 08 (2022) 001, and work in progress

2022 NCTS Annual Theory Meeting, 14-16 Dec. 2022

Introduction

- Higgs potential gives the mass to the SM particles through spontaneous symmetry breaking.

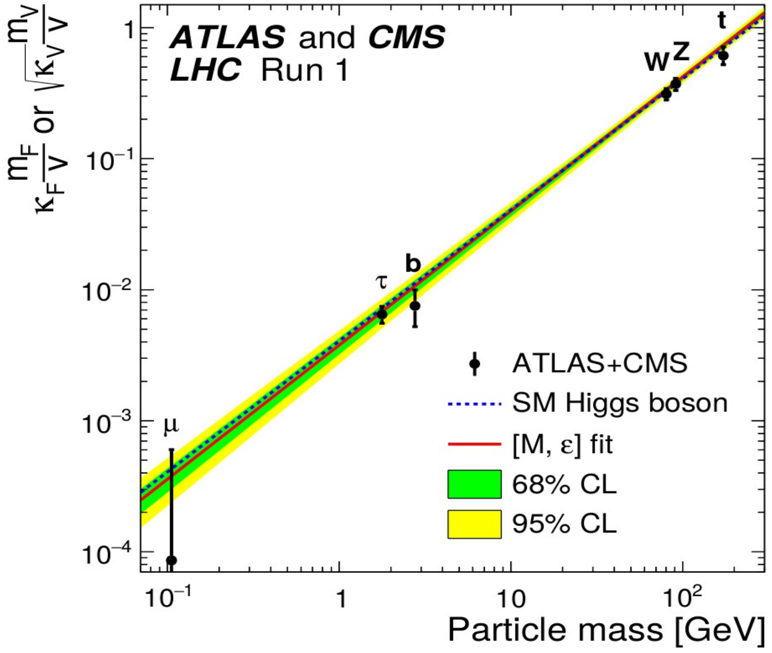

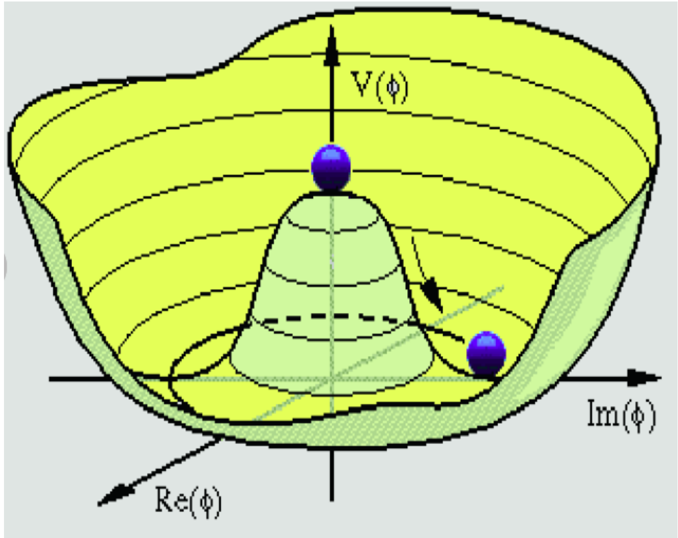

Dezso Horvath: Higgs and BSM studies at the LHC

Introduction

- The mass origin of dark fermion χ may come from the **spontaneous symmetry breaking** inducing by another scalar.

$$\mathcal{L} \supset \bar{\chi}(i\partial\!\!\!/ - m)\chi - g_\chi \phi \bar{\chi}\chi - V_{\rm eff}(\phi, T)$$

$$m_\chi = m + g_\chi v_\phi, \quad v_\phi \equiv \langle \phi \rangle$$

- We consider **1st order phase transition (FOPT)**.

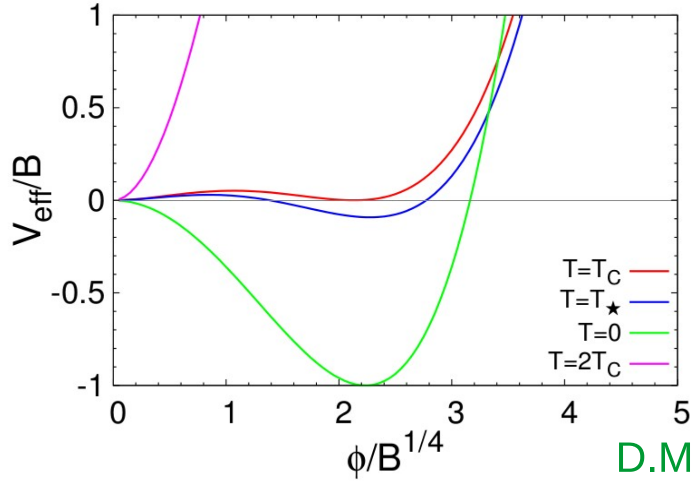

D.Marfatia, P.Y. Tseng: 2107.00859

Introduction

- More rich phenomenologies, if we consider **1st order phase transition (FOPT)**.

J.P.Hong, S.Jung, K.P.Xie: 2008.04430

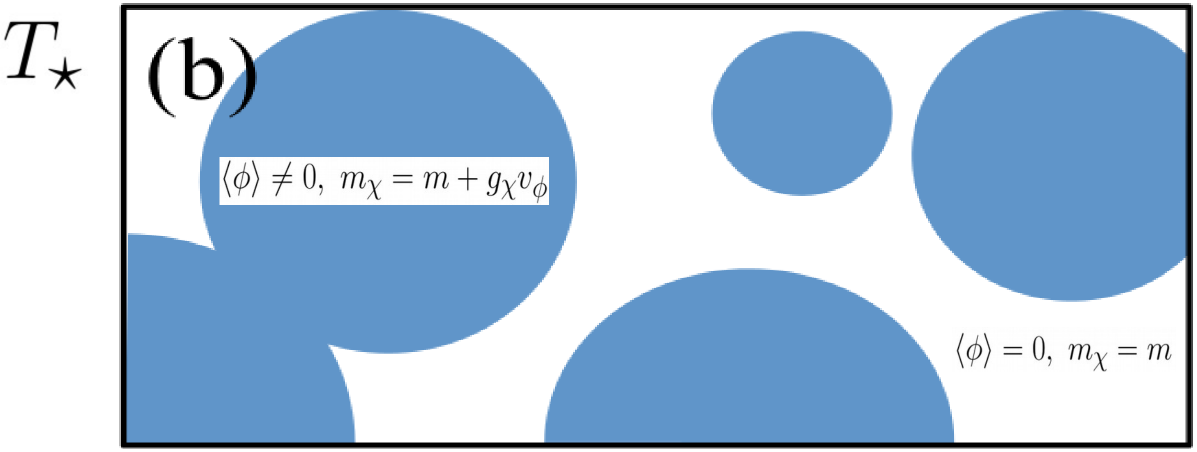

- Dark fermion χ **inside** the bubble becomes the DM relic density (bubble filtering χ).

- χ **outside** the bubble could form macroscopic DM (Fermi Ball or primordial black hole)

Introduction

- More rich phenomenologies, if we consider **1st order phase transition (FOPT)**.

K.Kawana, K.P.Xie: 2106.00111

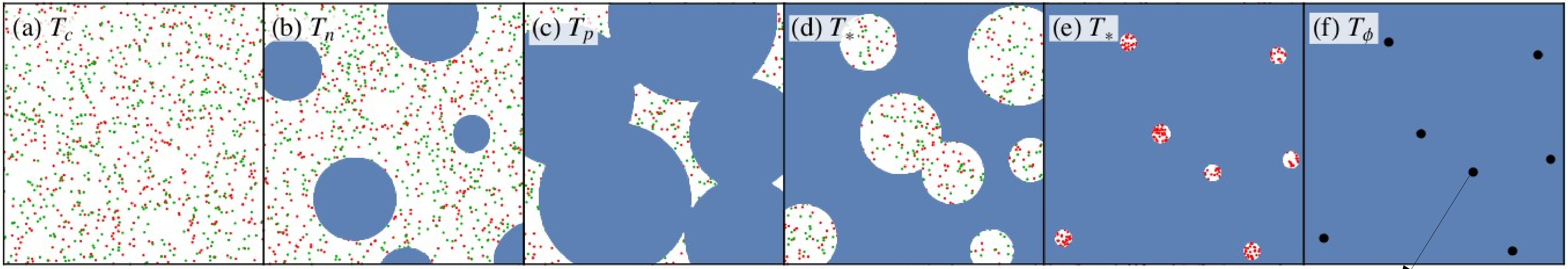

- Dark fermion χ **inside** the bubble becomes the DM relic density (bubble filtering χ).

- χ **outside** the bubble could form macroscopic DM (Fermi Ball or primordial black hole)

Bubble Wall

- During FOPT, lighter (heavier) χ locate outside (inside) the bubble, and momentum conservation much be satisfied at the bubble wall.

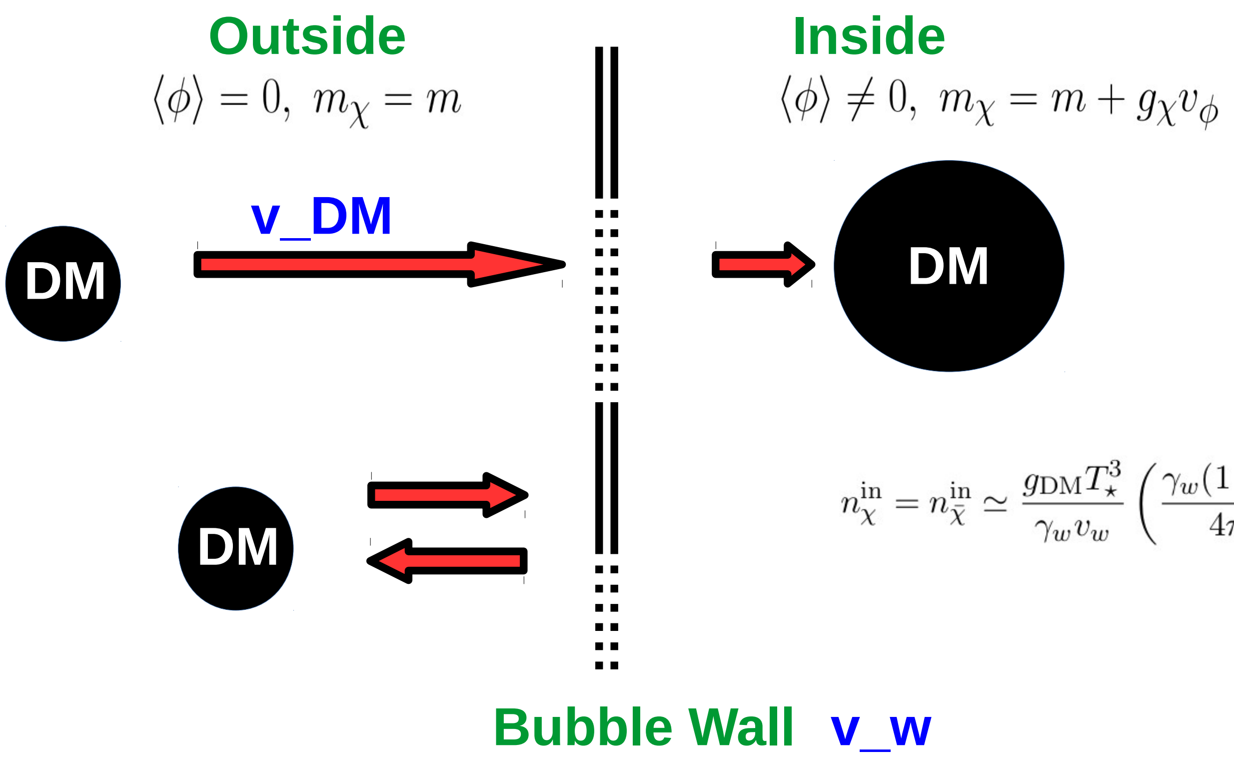

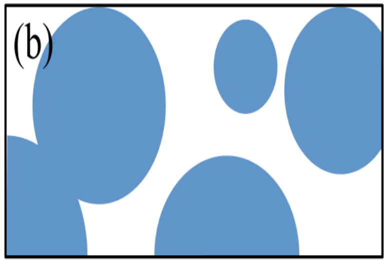

$$n_\chi^{\rm in} = n_{\bar\chi}^{\rm in} \simeq \frac{g_{\rm DM} T_\star^3}{\gamma_w v_w}\left(\frac{\gamma_w(1-v_w)m_\chi/T_\star + 1}{4\pi^2\gamma_\omega^3(1-v_w)^2}\right) e^{-\frac{\gamma_w(1-v_w)m_\chi}{T_\star}}$$

Bubble Wall

- Suppose χ particle mass difference is large: $\Delta m_\chi \simeq g_\chi v_\phi > T_c$
- χ particles, remaining in **outside** the bubble (trapped in the *false vacuum*), will be aggregated by the expanding bubbles and form a macroscopic **Fermi-Ball(FB)**.
- For this to occur, there must be non-zero **asymmetry** $\eta_\chi \equiv (n_\chi - n_{\bar{\chi}})/s$ in the false vacuum so that the an excess remain after pair annihilation.
- **FB** stability: $$\frac{dM_{\rm FB}}{dQ_{\rm FB}} < m + g_\chi v_\phi, \quad \text{and} \quad \frac{d^2 M_{\rm FB}}{dQ_{\rm FB}^2} < 0$$

Number density of FB

- FBs start to form at $T_\star$ in the false vacuum, it shrinks and separates into smaller volumes.
- Critical volume $V_\star = 4\pi R_\star^3/3$, there is no other bubble forming inside during its shrinking $\Gamma(T_\star)V_\star \Delta t \sim 1$, corresponds to one FB.
- The number density of FB $n_{\rm FB}|_{T_\star}$ is determined by $n_{\rm FB}|_{T_\star} V_\star = F(t_\star)$:

$$n_{\rm FB}|_{T_\star} = \left(\frac{3}{4\pi}\right)^{1/4} \left(\frac{\Gamma(T_\star)}{v_w}\right)^{3/4} F(t_\star)$$

- Total numbers of χ for a FB: $Q_{\rm FB} = \eta_\chi \left(\frac{s}{n_{\rm FB}}\right)_{T_\star}$

FB mass profile

- The mass and radius of FB are obtained by minimizing the FB energy with respect to the radius $dE_{\rm FB}/dR = 0$:

$$E_{\rm FB} = \frac{3\pi}{4}\left(\frac{3}{2\pi}\right)^{2/3}\frac{Q_{\rm FB}^{4/3}}{R}\left[1+\frac{4\pi}{9}\left(\frac{2\pi}{3}\right)^{1/3}\frac{R^2T^2}{Q_{\rm FB}^{2/3}}\right] - \frac{3g_\chi^2}{8\pi}\frac{Q_{\rm FB}^2 L_\phi^2}{R^3} + \frac{4\pi}{3}V_0(T)R^3$$

$$R_{\rm FB} = \left[\frac{3}{16}\left(\frac{3}{2\pi}\right)^{2/3}\frac{Q_{\rm FB}^{4/3}}{V_0}\right]^{1/4}\left[1-\frac{\pi}{6\sqrt{3}}\frac{T^2}{V_0^{1/2}}\right]^{1/2},$$

$$M_{\rm FB} = Q_{\rm FB}\,(12\pi^2 V_0)^{1/4}\left(1+\frac{\pi}{4\sqrt{3}}\frac{T^2}{V_0^{1/2}}\right),$$

- FB relic abundance: $\Omega_{\rm FB}h^2 = \dfrac{M_{\rm FB}\, n_{\rm FB}|_{T_0}}{3M_{\rm Pl}^2(H_0/h)^2}$

FB collapse to PBH

- The mass and radius of FB are obtained by minimizing the FB energy with respect to the radius $dE_{\rm FB}/dR = 0$:

$$E_{\rm FB} = \frac{3\pi}{4}\left(\frac{3}{2\pi}\right)^{2/3}\frac{Q_{\rm FB}^{4/3}}{R}\left[1+\frac{4\pi}{9}\left(\frac{2\pi}{3}\right)^{1/3}\frac{R^2T^2}{Q_{\rm FB}^{2/3}}\right] - \frac{3g_\chi^2}{8\pi}\frac{Q_{\rm FB}^2 L_\phi^2}{R^3} + \frac{4\pi}{3}V_0(T)R^3$$

$$L_\phi(T) \equiv \left(\frac{d^2V_{\rm eff}}{d\phi^2}\bigg|_{\phi=0}\right)^{-1/2} = \left(2D(T^2-T_0^2)\right)^{-1/2}$$

- Magnitude of Yukawa energy increases as FB temperature decrease. It will dominate when $L_\phi \simeq R_{\rm FB}/Q_{\rm FB}^{1/3}$, and FB collapse to PBH.

FB collapse to PBH

- Bounds on the PBH fraction of the energy density when they form are placed in term of

D.Marfatia, P.Y.Tseng: 2112.14588

$$\beta' \equiv 4.58 \times 10^{-12} \frac{T_\phi}{\mathrm{MeV}} \left(\frac{M_{\mathrm{PBH}}}{10^{-18} M_\odot} \right)^{1/2} \frac{\rho_{\mathrm{PBH}}(T_\phi)}{\rho(T_\phi)}$$

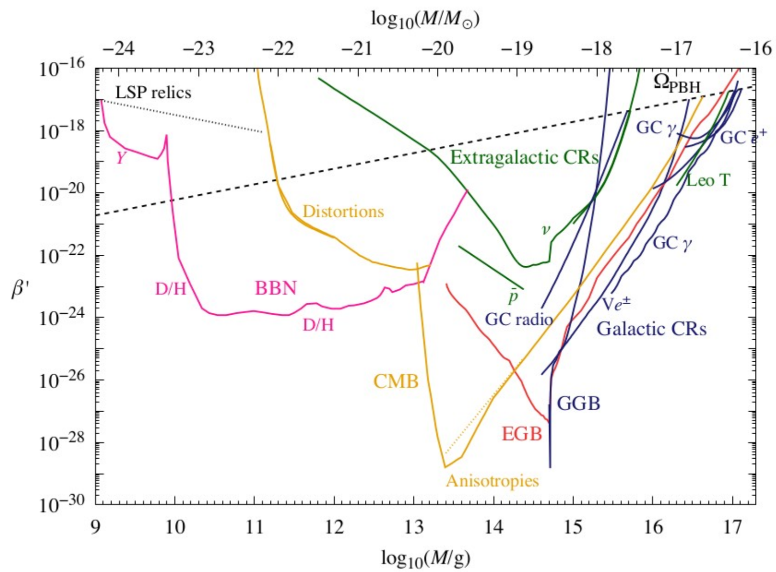

B.Carr, K.Kohri,Y.Sendouda,J.Yokoyama: 2002.12778

Quartic effective potential

- We consider the finite-temperature quartic effective potential induce the FOPT:

$$V_{\text{eff}}(\phi, T) = D(T^2 - T_0^2)\phi^2 - (AT + C)\phi^3 + \frac{\lambda}{4}\phi^4$$

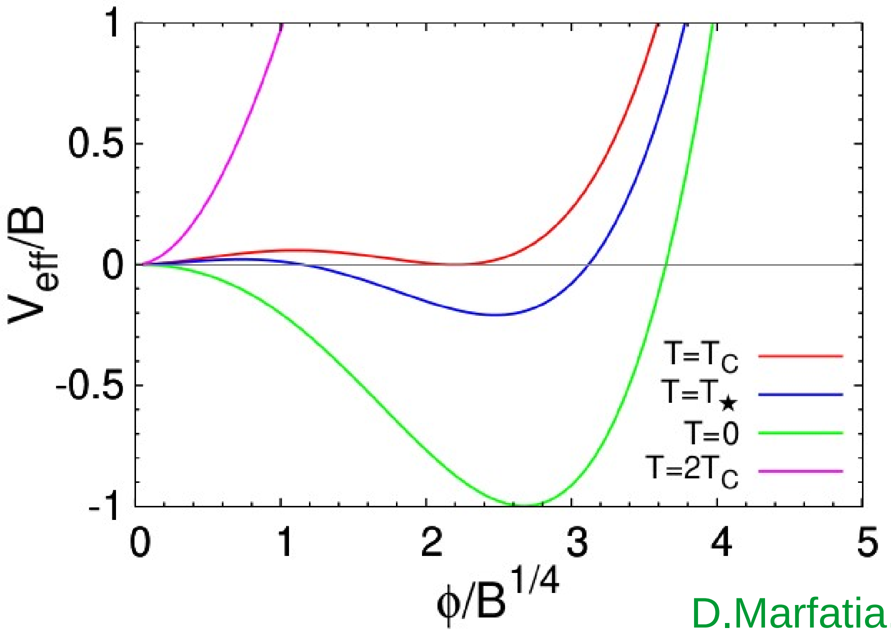

D.Marfatia, P.Y. Tseng: 2107.00859

Dark fermion evaporated from PBH

Dark fermion flux from PBH evaporation

- Hawking temperature characterizes black-body spectrum from PBH evaporation:

BlackHawk v2.1, A.Aarbey, J.Auffinger: 2108.02737

$$T_{\rm PBH} \simeq 5.3~{\rm MeV} \times \left(\frac{10^{-18} M_\odot}{M_{\rm PBH}}\right)$$

$$\frac{dN_\chi}{d\mathcal{T}dt} = \frac{2\Gamma_\chi(\mathcal{T}, M_{\rm PBH})}{\pi(e^{(\mathcal{T}+m_\chi)/T_{\rm PBH}}+1)}$$

- χ flux on Earth come from extragalactic PBH, it does not rely on DM density near galactic center

$$\frac{d\Phi}{d\mathcal{T}} = \int_{t_\phi}^{\min(t_{\rm eva}, t_0)} c\,dt[1+z(t)]\frac{f_{\rm PBH}\rho_{\rm DM}}{M_{\rm PBH}}\frac{d^2N_\chi}{d\mathcal{T}dt}\bigg|_{\tilde{E}=\sqrt{(E^2-m_\chi^2)(1+z(t))^2+m_\chi^2}}$$

R.Calabrese et. al: 2203.17093

Signals from PBH

DM-e scattering

- We are interested in χ in energy range from keV to GeV so that XENON1T/XENONnT and SK/HK can detect a signal.

$$\frac{d\sigma}{dE_r} = \frac{\sigma_{\chi e}\Theta(E_r^{\max} - E_r)}{8\mu_{\chi e}^2 \tilde{p}^2}(2m_e + E_r)(2m_\chi^2 + m_e E_r)$$

- The maximum allowed recoil energy

$$E_r^{\max} = \frac{2m_e \mathcal{T}(\mathcal{T} + 2m_e)}{((m_e + m_\chi)^2 + 2m_e \mathcal{T})}$$

At XENON1T/XENONnT

- At XENON1T/XENONnT detector, χ can ionize the Xe atom via $\chi + \text{Xe} \rightarrow \chi + \text{Xe}^* + e^-$, which produces an electron recoil signal.

XENON Collaboration: 2207.11330, 2006.09721

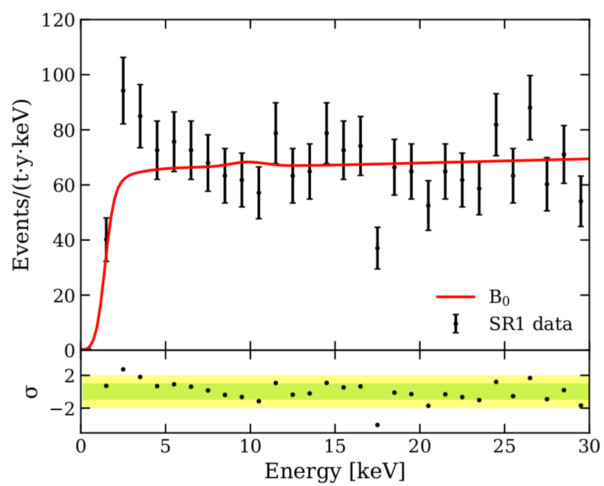

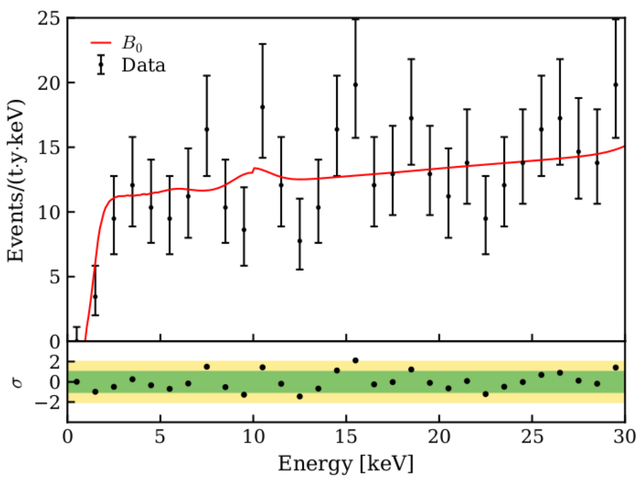

- XENONnT reduced tritium background five times lower than in XENON1T.

At XENON1T/XENONnT

- At XENON1T/XENONnT detector, the differential event rate is given by

$$\frac{dR}{dE_r} = n_t\, \eta(E_r)\, \tilde{F}(E_r) \int d\mathcal{T} \frac{d\Phi}{d\mathcal{T}} \sum_{n,l} \frac{d\sigma^{n,l}}{dE_r}$$

including the cross section of scattering of χ on a bound electron, because the binding energy is non-negligible compared to energy of χ .

R.Calabrese et. al: 2203.17093

- To find parameter space allowed by data

$$\chi^2 \equiv \sum_i \left(\frac{\left.\frac{dR}{dE_r}\right|_i + \left.\frac{dR_{\rm bkgd}}{dE_r}\right|_i - \left.\frac{dR_{\rm obs}}{dE_r}\right|_i}{\sigma_i} \right)^2$$

At SK/HK

- At SK/HK, χ-e scattering produce Cherenkov radiation.
- 161.9 kiloton-year SK observed 4042 events , which is compatible with background 3992.9. Super-Kamiokande: 1711.05278

$$N_{\rm PBH}^{\rm SK} = 161.9\ [\rm kton - yr] \times \int_{0.1\ \rm GeV}^{1.33\ \rm GeV} dE_r \frac{dR}{dE_r}$$

- Define 2σ exclusion by $N_{\rm PBH}^{\rm SK} / \sqrt{N_{\rm PBH}^{\rm SK} + N_{\rm bkgd}^{\rm SK}} \geq 2$.
- HK is expected to collect 3.74 Mton-year exposure.

Hyper-Kamiokande: 1805.04163

Correlated signals

Parameter scan

- Parametrization of quartic effective potential:

$$V_{\rm eff}(\phi,T) = D(T^2 - T_0^2)\phi^2 - (AT + C)\phi^3 + \frac{\lambda}{4}\phi^4$$

- Ranges of parameter scan:

$$0.05 \le \lambda \le 0.2\,, \quad 0.1 \le B^{1/4}/\mathrm{MeV} \le 10^4\,, \quad 0.01 \le C/\mathrm{MeV} \le 10^4\,,$$
$$0.1 \le D \le 10\,, \quad 0.3 \le T_\star/T_{\mathrm{SM}\star} \le 1.0\,, \quad 0.01 \le g_\chi \le \sqrt{4\pi}\,,$$
$$10^{-3} \le m/B^{1/4} \le 10\,, \quad 10^{-40} \le \sigma_{\chi e}/\mathrm{cm}^2 \le 10^{-31}\,.$$

Parameter scan

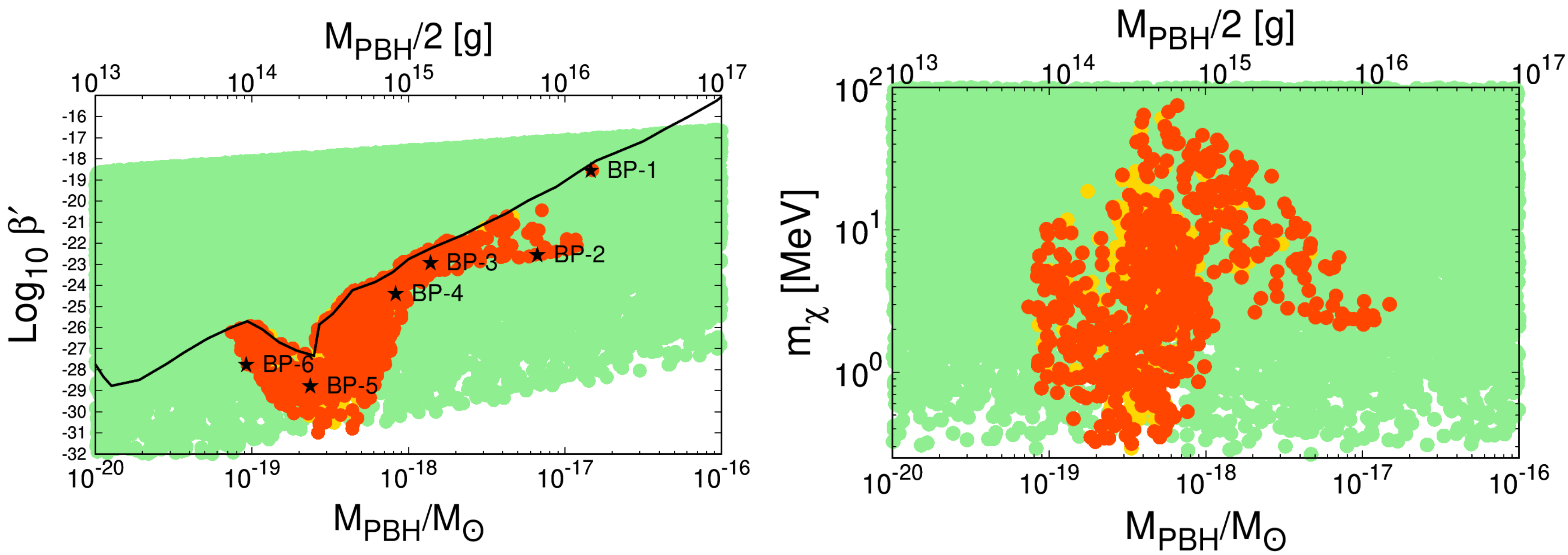

Figure 1. The regions of parameter space that produce a detectable boosted DM flux at XENON1T/XENONnT/SK+GW (yellow), XENONnT/HK+GW (red), and a gravitational wave signal at THEIA/μAres (green).

Parameter scan

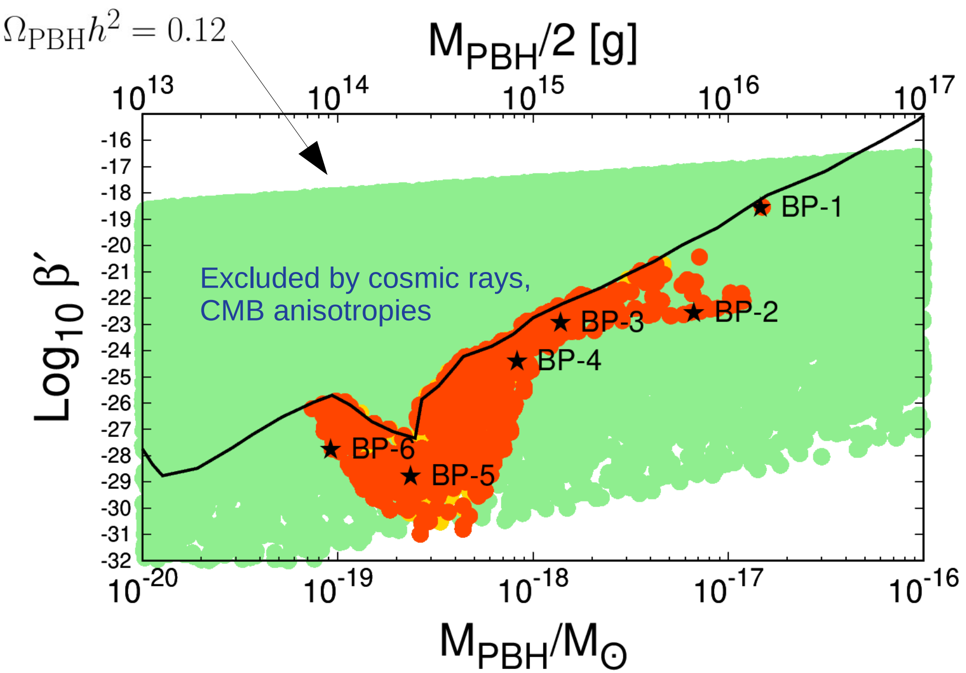

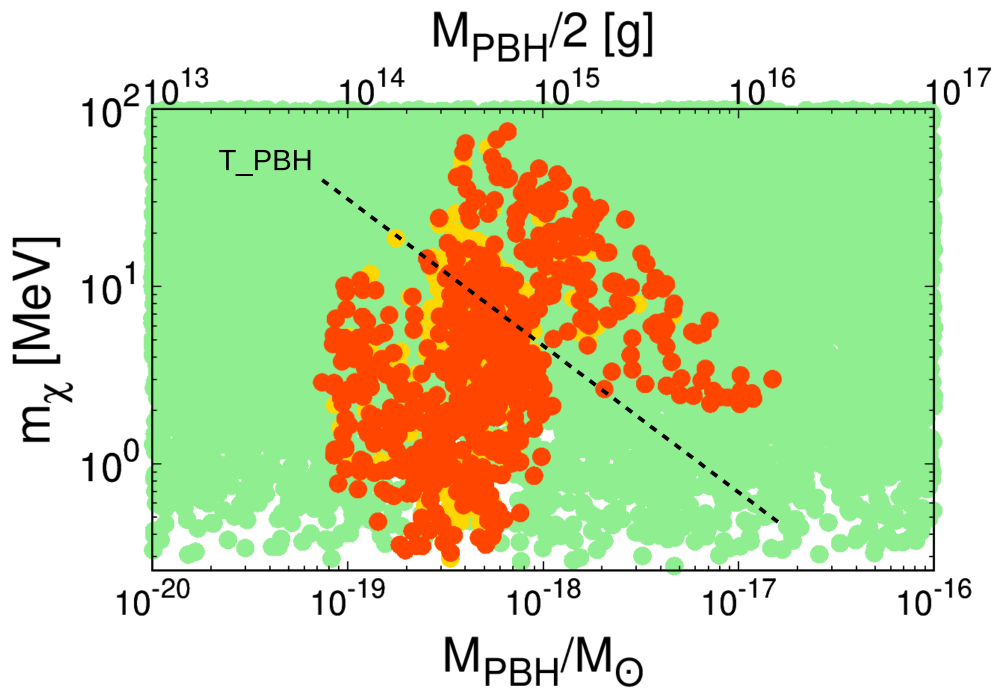

Figure 1. The regions of parameter space that produce a detectable boosted DM flux at XENON1T/XENONnT/SK+GW (yellow), XENONnT/HK+GW (red), and a gravitational wave signal at THEIA/μAres (green).

Parameter scan

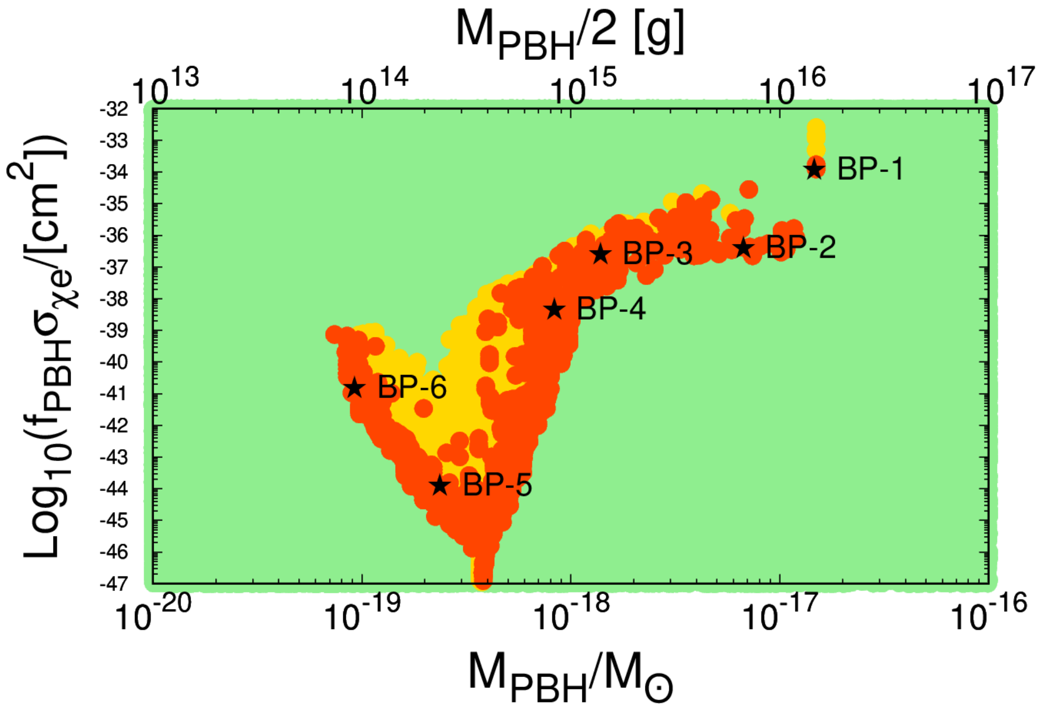

Figure 1. The regions of parameter space that produce a detectable boosted DM flux at XENON1T/XENONnT/SK+GW (yellow), XENONnT/HK+GW (red), and a gravitational wave signal at THEIA/μAres (green).

Parameter scan

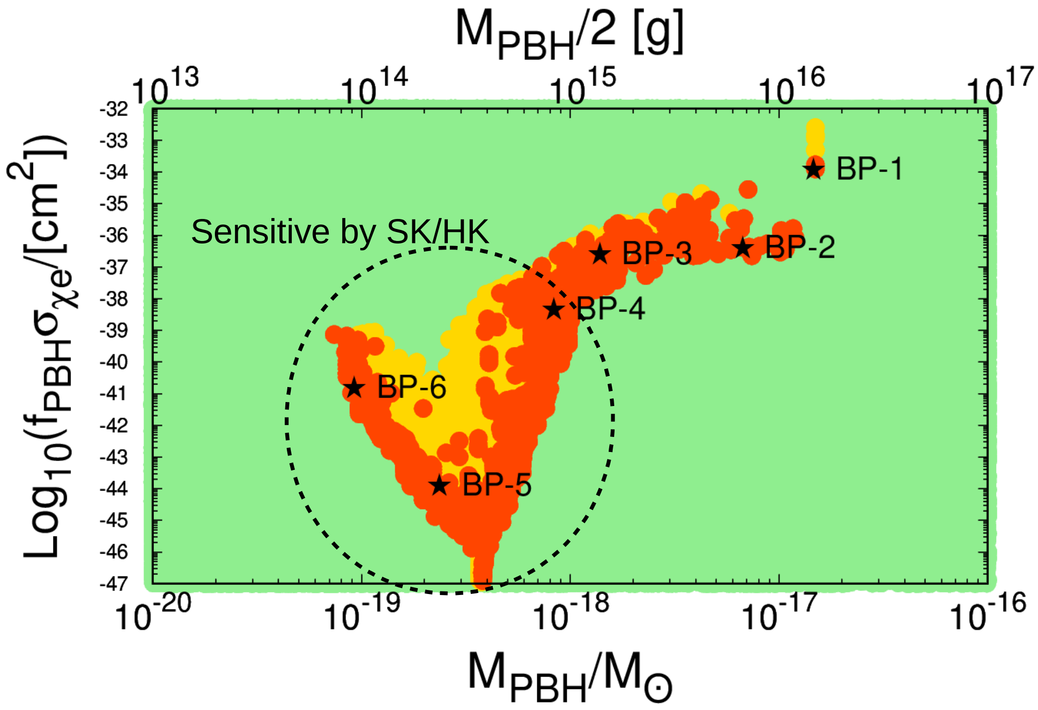

Figure 1. The regions of parameter space that produce a detectable boosted DM flux at XENON1T/XENONnT/SK+GW (yellow), XENONnT/HK+GW (red), and a gravitational wave signal at THEIA/μAres (green).

Parameter scan

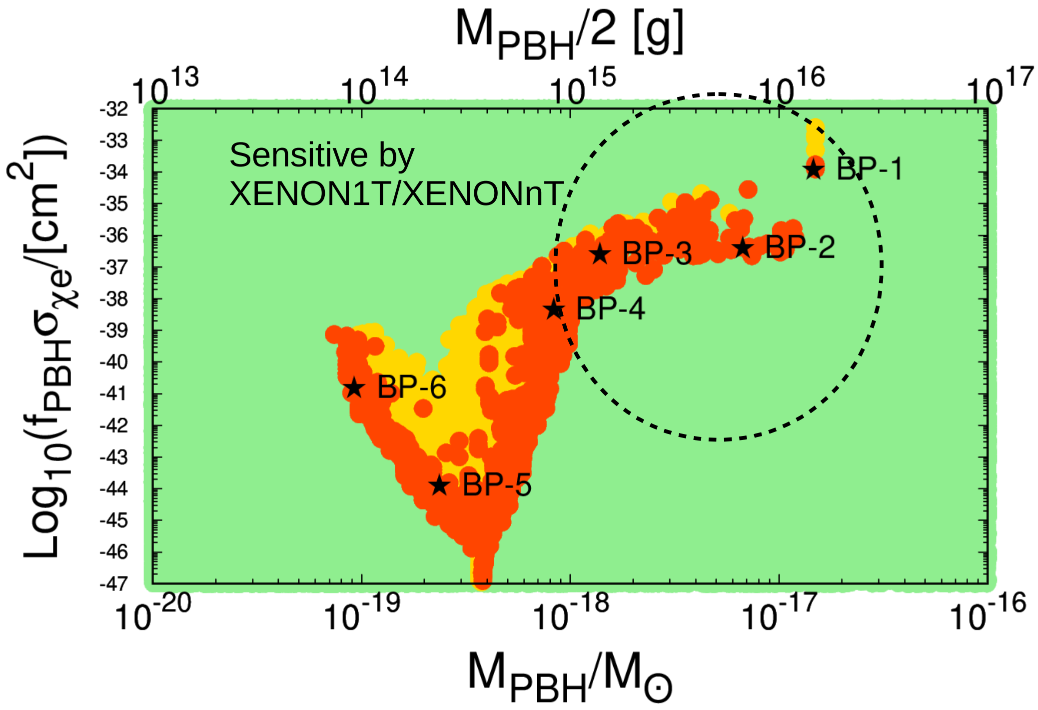

Figure 1. The regions of parameter space that produce a detectable boosted DM flux at XENON1T/XENONnT/SK+GW (yellow), XENONnT/HK+GW (red), and a gravitational wave signal at THEIA/μAres (green).

Discussion: FB stability

- The stable conditions for FBs not decay to χ or fission to lighter FBs

$$\frac{dM_{\rm FB}}{dQ_{\rm FB}} < m + g_\chi v_\phi, \quad \text{and} \quad \frac{d^2 M_{\rm FB}}{dQ_{\rm FB}^2} < 0$$

- χ-e scattering, the χ may be ejected from FB unless its mean free path is short enough that multiple scattering with other χ in the FB slows it down.

- The χ-χ scattering $\sigma_{\chi\chi}$ via ϕ is larger than $\sigma_{\chi e} < 10^{-31}\ {\rm cm}^2$. The $\ell_\chi \equiv (n_\chi \sigma_{\chi\chi})^{-1}$ is much smaller than $R_{\rm FB}$.

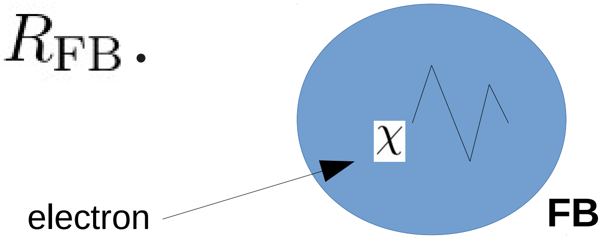

Discussion: relic of dark scalar

- During FB formation, ϕ can be copiously produced via $\chi\bar{\chi} \to \phi\phi$. Since ϕ is non-relativistic and evolve like matter, so that its relic density may overclose the Universe.

- To avoid this, we allow ϕ decay to a pair of relativistic scalars s, which preserves the relativistic degree of freedom in dark sector. We require $\Delta N_{\rm eff} \leq 0.5$.

- The trilinear term $\mu\phi s s$

$$\tau_{\phi\to ss} \simeq 6.6 \times 10^{-20} \left(\frac{\rm MeV}{\mu}\right)^2 \left(\frac{m_\phi}{\rm MeV}\right) \;\; [\rm sec]$$

Summary

Summary

- We combined the PBH production from cosmological FOPT and χ's evaporated from PBH, provides a mechanism to boost extragalactic χ flux.
- We found $0.1 \lesssim B^{1/4}/\mathrm{MeV} \lesssim 10$ of FOPT incorporating $0.1 \lesssim m_\chi/\mathrm{MeV} \lesssim 100$ generates $2 \times 10^{-20} \lesssim M_{\mathrm{PBH}}/M_\odot \lesssim 4 \times 10^{-17}$, whose Hawking temperature is high enough to reproduce χ from its evaporation.
- Further assume χ-e cross section, the extragalatic χ flux scattering with the electrons inside the XENON1T/XENONnT and SuperK/HyperK detectors.

Summary

- XENON1T/XENONnT represent low threshold experiments, meanwhile SK/HK correspond with large exposure detectors.

- XENON1T/XENONnT are sensitive to $M_{\rm PBH}/M_\odot \gtrsim 10^{-18}$ or $m_\chi \gtrsim 5~{\rm MeV}$, and SK/HK can probe small $f_{\rm PBH} \times \sigma_{\chi e}$ values.

Thank you for your attention!

Back up

Signals from FB

Fermi ball

- We consider the finite-temperature quartic effective potential:

D.Marfatia, P.Y. Tseng: 2107.00859

Table 1. Benchmark points with $A = 0.1$. $N_{\rm events}$ is the number of microlensing events expected in 70 hours of observation of M31 by Subaru-HSC.

	BP-1	BP-2	BP-3	BP-4	BP-5	BP-6	BP-7	BP-8
λ	0.134	0.158	0.193	0.078	0.062	0.072	0.053	0.060
$B^{1/4}$/keV	2.42	43.5	34.9	64.2	63.6	73.2	284	1390
C/keV	0.059	6.234	4.988	3.080	0.315	0.586	0.342	7.713
D	5.807	0.451	0.720	0.445	0.257	0.293	0.584	0.706
η_χ	7.34×10^{-6}	1.37×10^{-7}	3.51×10^{-6}	4.55×10^{-8}	6.98×10^{-9}	3.64×10^{-9}	8.54×10^{-9}	2.40×10^{-8}
$T_{\rm SM\star}$/keV	1.41	100.0	64.5	128.1	164.8	169.5	427.8	1601
$T_\star$/keV	0.57	34.2	21.6	52.3	84.8	86.9	201.0	879.0
T_f/keV	0.63	41.4	25.9	64.4	92.9	92.5	233.2	1005
$S_3(T_\star)/T_\star$	189	188	187	186	187	184	177	171
$M_{\rm FB}/M_\odot$	3.37×10^{-6}	1.11×10^{-6}	9.66×10^{-6}	1.01×10^{-7}	1.08×10^{-8}	1.08×10^{-9}	9.66×10^{-11}	1.09×10^{-11}
$R_{\rm FB}/R_\odot$	0.529	7.77×10^{-3}	2.15×10^{-2}	2.09×10^{-3}	1.00×10^{-3}	3.86×10^{-4}	2.83×10^{-5}	1.64×10^{-6}
$Q_{\rm FB}$	4.70×10^{56}	8.62×10^{54}	9.38×10^{55}	5.34×10^{53}	5.74×10^{52}	5.00×10^{51}	1.15×10^{50}	2.65×10^{48}
α	1.63×10^{-2}	1.56×10^{-2}	1.70×10^{-2}	2.83×10^{-2}	2.00×10^{-2}	1.24×10^{-2}	1.79×10^{-2}	2.62×10^{-2}
$\beta/H_\star$	3.43×10^4	1.57×10^3	3.01×10^3	2.04×10^3	1.86×10^3	2.80×10^3	4.44×10^3	5.59×10^3
$v_\phi/T_\star$	3.554	4.175	3.958	4.889	3.987	3.501	4.724	4.469
v_w	0.890	0.940	0.937	0.946	0.886	0.854	0.923	0.916
$\Omega_{\rm FB}h^2$	1.79×10^{-2}	5.81×10^{-3}	0.12	2.94×10^{-3}	4.56×10^{-4}	2.70×10^{-4}	2.39×10^{-3}	3.38×10^{-2}
$N_{\rm events}$	19.5	20.4	29.3	38.9	17.5	19.3	46.1	29.1
$\Delta N_{\rm eff}$	0.391	0.226	0.248	0.394	0.497	0.425	0.261	0.408

Microlensing

Microlensing

- These FB mass and radius ranges can induce microlensing effects.

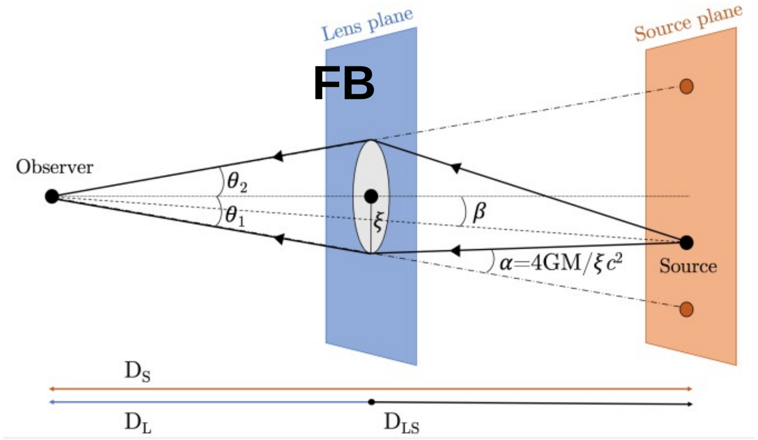

$$\theta_E \equiv \sqrt{\frac{4GM}{c^2}\frac{D_{LS}}{D_L D_S}}$$

$$\mu_{tot} = \frac{u^2+2}{u\sqrt{u^2+4}} \xrightarrow{u=1} 1.34 \, .$$

D.Croon, D. McKeen, N. Raj: 2002.08962

- The separating angle of two images of the background star are too small to be resolved, but we can observe the sudden luminosity enhancement of the star.

Microlensing

- Astrophysical Sky surveys are ideal for observing microlensing. Ex. Subaru-HSC (observing M31 for 7 hrs).

FB halos surround MW and M31. FBs and stars have relative velocity of 250 km/s.

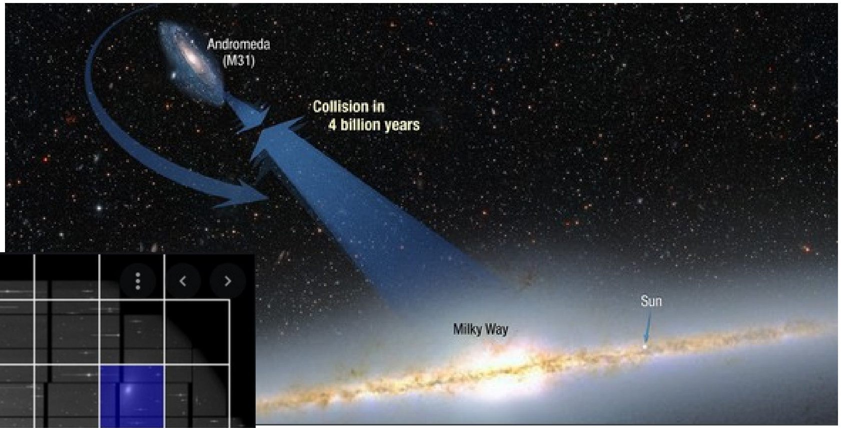

Milky Way Destined for Head-On Collision | NASA

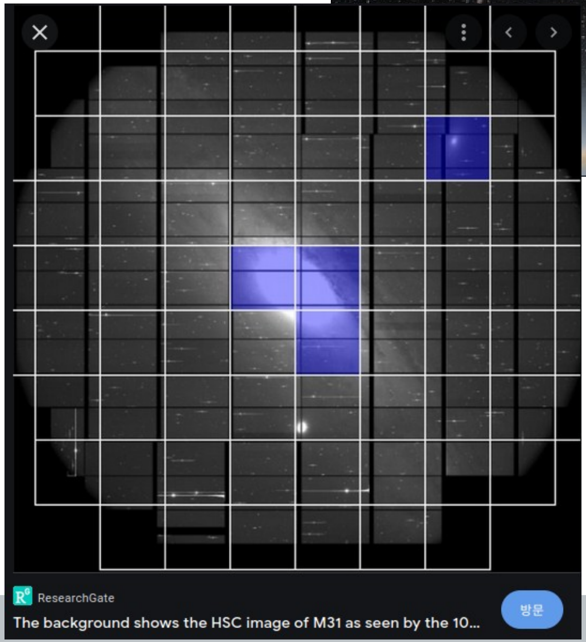

M31 image from Subaru-HSC

Microlensing

- If the lenses have a universal mass $M_{\rm FB}$, with Maxwell-Boltzmann velocity distribution, then event rate per source star is

$$\frac{d^2\Gamma}{dx dt_E} = D_S \frac{f_{\rm DM}}{M_{\rm FB}} \left[\rho^{\rm DM}_{\rm MW}(r_{\rm MW}) \frac{v_E^4}{v_{\rm MW}^2} e^{-v_E^2/v_{\rm MW}^2} + \rho^{\rm DM}_{\rm M31}(r_{\rm M31}) \frac{v_E^4}{v_{\rm M31}^2} e^{-v_E^2/v_{\rm M31}^2} \right]$$

$$v_E(x) = 2u_{1.34}(x) R_E(x)/t_E$$

- The t_E is the time duration for each event.

$$x \equiv D_L/D_S$$

u1.34=1 for point-like lens and background star.

Microlensing

- If the lenses have a universal mass $M_{\rm FB}$, with Maxwell-Boltzmann velocity distribution, then event rate per source star is

$$\frac{d^2\Gamma}{dx\,dt_E} = D_S \frac{f_{\rm DM}}{M_{\rm FB}} \left[\rho^{\rm DM}_{\rm MW}(r_{\rm MW}) \frac{v_E^4}{v_{\rm MW}^2} e^{-v_E^2/v_{\rm MW}^2} + \rho^{\rm DM}_{\rm M31}(r_{\rm M31}) \frac{v_E^4}{v_{\rm M31}^2} e^{-v_E^2/v_{\rm M31}^2}\right]$$

$$v_E(x) = 2u_{1.34}(x) R_E(x)/t_E$$

- The radius distribution of stars in M31:

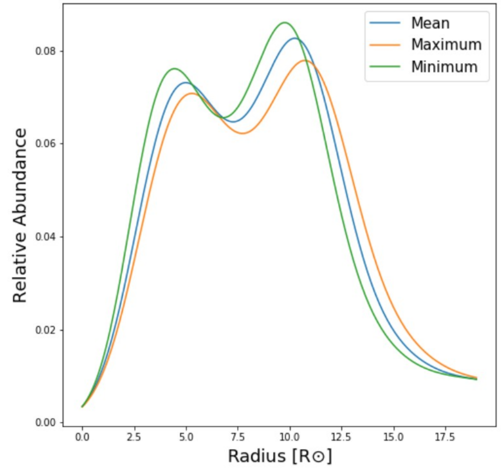

N.Smyth et.al: 1910.01285

Microlensing: Finite-size

- Finite-size effect:

D.Croon, D.McKeen, N.Raj, and Z.Wang: 2007.12697

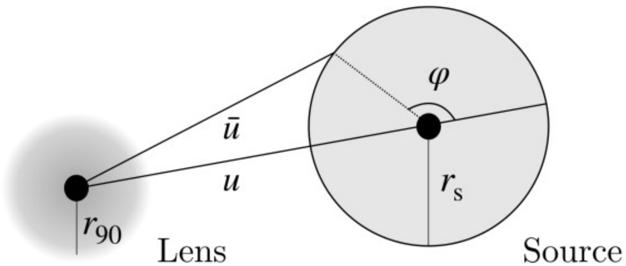

$$\bar{u}(\varphi) = \sqrt{u^2 + r_S^2 + 2ur_S\cos\varphi}$$

- Solve the lens equation along the edge of the source:

$$\bar{u}(\varphi) = t(\varphi) - \frac{m(t(\varphi))}{t(\varphi)}$$

- The magnification is the area of each image:

$$\mu_i = \eta\frac{1}{\pi r_S^2}\int_0^\pi t_{\varphi,i}^2(\psi)d\psi$$

$$\psi = \tan^{-1}\frac{r_S\sin\varphi}{u + r_S\cos\varphi}, \quad 0 \leq \psi \leq \pi$$

Microlensing: Finite-size

- Finite-size effect:

D.Croon, D.McKeen, N.Raj, and Z.Wang: 2007.12697

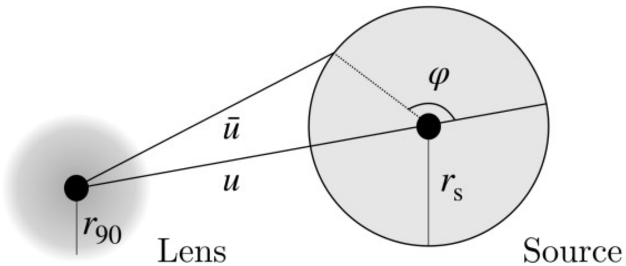

$$\bar{u}(\varphi) = \sqrt{u^2 + r_S^2 + 2ur_S\cos\varphi}$$

- The effective size for 1.34 times magnification:

$$\mu_{\rm tot}(u \le u_{1.34}) \ge 1.34$$

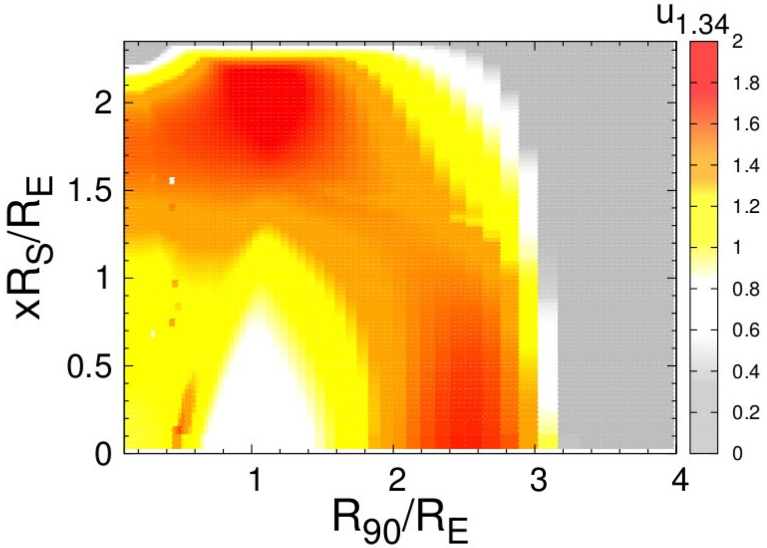

D.Marfatia, P.Y. Tseng: 2107.00859

Microlensing: Finite-size

- If the lenses have a universal mass $M_{\rm FB}$, with Maxwell-Boltzmann velocity distribution, then event rate per source star is

$$\frac{d^2\Gamma}{dx dt_E} = D_S \frac{f_{\rm DM}}{M_{\rm FB}} \left[\rho^{\rm DM}_{\rm MW}(r_{\rm MW}) \frac{v_E^4}{v_{\rm MW}^2} e^{-v_E^2/v_{\rm MW}^2} + \rho^{\rm DM}_{\rm M31}(r_{\rm M31}) \frac{v_E^4}{v_{\rm M31}^2} e^{-v_E^2/v_{\rm M31}^2} \right]$$

$$v_E(x) = 2u_{1.34}(x) R_E(x)/t_E$$

- Finite-size effect:

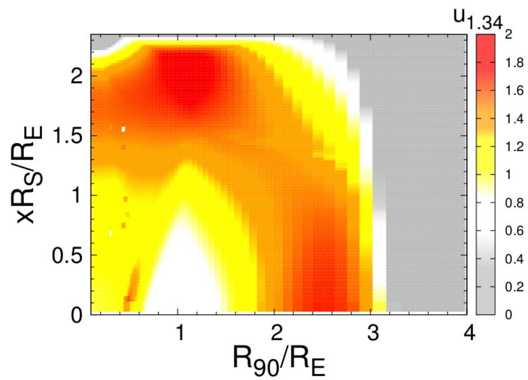

D.Marfatia, P.Y. Tseng: 2107.00859

Microlensing

- If the lenses have a universal mass $M_{\rm FB}$, with Maxwell-Boltzmann velocity distribution, then event rate per source star is

$$\frac{d^2\Gamma}{dx\,dt_E} = D_S \frac{f_{\rm DM}}{M_{\rm FB}}\left[\rho^{\rm DM}_{\rm MW}(r_{\rm MW})\frac{v_E^4}{v^2_{\rm MW}}e^{-v_E^2/v^2_{\rm MW}} + \rho^{\rm DM}_{\rm M31}(r_{\rm M31})\frac{v_E^4}{v^2_{\rm M31}}e^{-v_E^2/v^2_{\rm M31}}\right]$$

- Total event rate, we need to sum over the stars in M31

$$N_{\rm events} = N_S T_{\rm obs}\int dt_E \int dR_S \int_0^1 dx \frac{d^2\Gamma}{dx\,dt_E}\frac{dn}{dR_S}$$

$$N_S = 8.7\times 10^7$$

$$T_{\rm obs} = 7\ \rm hrs$$

Microlensing

- The 95% CL on the fractional FB relic abundance $f_{\rm DM}$ requiring $N_{\rm event} \leq 4.74$ corresponds to one observed event at Subaru-HSC:

$$10^{-12} M_\odot \lesssim M_{\rm FB} \lesssim 10^{-5} M_\odot$$

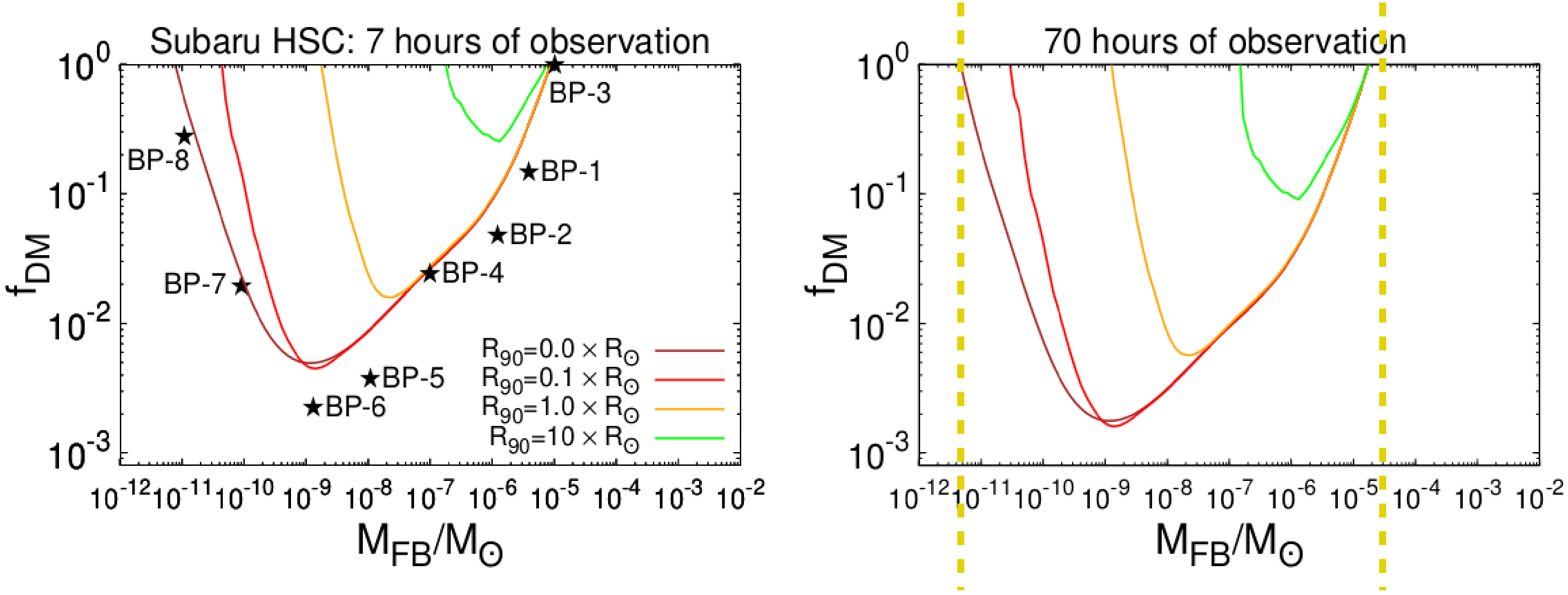

Here we included the finite size effect for microlensing.

Relativistic degree of freedom

- The temperature of FOPT is lower than the BBN, and robust 95% CL upper limit is $\Delta N_{\rm eff} \lesssim 0.5$. 2009.09745, 1103.1261

Table 1. Benchmark points with $A = 0.1$. $N_{\rm events}$ is the number of microlensing events expected in 70 hours of observation of M31 by Subaru-HSC.

Temperature of FOPT

	BP-1	BP-2	BP-3	BP-4	BP-5	BP-6	BP-7	BP-8
λ	0.134	0.158	0.193	0.078	0.062	0.072	0.053	0.060
$B^{1/4}$/keV	2.42	43.5	34.9	64.2	63.6	73.2	284	1390
C/keV	0.059	6.234	4.988	3.080	0.315	0.586	0.342	7.713
D	5.807	0.451	0.720	0.445	0.257	0.293	0.584	0.706
η_χ	7.34×10^{-6}	1.37×10^{-7}	3.51×10^{-6}	4.55×10^{-8}	6.98×10^{-9}	3.64×10^{-9}	8.54×10^{-9}	2.40×10^{-8}
$T_{\rm SM\star}$/keV	1.41	100.0	64.5	128.1	164.8	169.5	427.8	1601
$T_\star$/keV	0.57	34.2	21.6	52.3	84.8	86.9	201.0	879.0
T_f/keV	0.63	41.4	25.9	64.4	92.9	92.5	233.2	1005
$S_3(T_\star)/T_\star$	189	188	187	186	187	184	177	171
$M_{\rm FB}/M_\odot$	3.37×10^{-6}	1.11×10^{-6}	9.66×10^{-6}	1.01×10^{-7}	1.08×10^{-8}	1.08×10^{-9}	9.66×10^{-11}	1.09×10^{-11}
$R_{\rm FB}/R_\odot$	0.529	7.77×10^{-3}	2.15×10^{-2}	2.09×10^{-3}	1.00×10^{-3}	3.86×10^{-4}	2.83×10^{-5}	1.64×10^{-6}
$Q_{\rm FB}$	4.70×10^{56}	8.62×10^{54}	9.38×10^{55}	5.34×10^{53}	5.74×10^{52}	5.00×10^{51}	1.15×10^{50}	2.65×10^{48}
α	1.63×10^{-2}	1.56×10^{-2}	1.70×10^{-2}	2.83×10^{-2}	2.00×10^{-2}	1.24×10^{-2}	1.79×10^{-2}	2.62×10^{-2}
$\beta/H_\star$	3.43×10^4	1.57×10^3	3.01×10^3	2.04×10^3	1.86×10^3	2.80×10^3	4.44×10^3	5.59×10^3
$v_\phi/T_\star$	3.554	4.175	3.958	4.889	3.987	3.501	4.724	4.469
v_w	0.890	0.940	0.937	0.946	0.886	0.854	0.923	0.916
$\Omega_{\rm FB}h^2$	1.79×10^{-2}	5.81×10^{-3}	0.12	2.94×10^{-3}	4.56×10^{-4}	2.70×10^{-4}	2.39×10^{-3}	3.38×10^{-2}
$N_{\rm events}$	19.5	20.4	29.3	38.9	17.5	19.3	46.1	29.1
$\Delta N_{\rm eff}$	0.391	0.226	0.248	0.394	0.497	0.425	0.261	0.408

Gravitational Wave

Gravitational wave production

- A FOPT generates GWs from three processes: I). Bubble collisions, II). Sound wave in the plasma, III) Magnetohydrodynamic (MHD) turbulence.

- The relevant parameters are required to calculate the GW signals:

$$\begin{cases} T_\star\,, \\ \alpha \equiv \dfrac{\left(1 - T\frac{\partial}{\partial T}\right)\Delta V_{\rm eff}|_{T_\star}}{\rho(T_\star)}\,, \quad \rho \equiv \pi^2 g_\star T^4/30 \\ \dfrac{\beta}{H_\star} \simeq T_\star \dfrac{d(S_3/T)}{dT}\Big|_{T_\star} \\ v_w \end{cases}$$

Gravitational wave production

- A FOPT generates GWs from three processes: I). Bubble collisions, II). Sound wave in the plasma, III) Magnetohydrodynamic (MHD) turbulence.

- The Euclidean action:

$$S_3(T) = 4\pi \int_0^\infty r^2 dr \left[\frac{1}{2} \left(\frac{d\phi}{dr} \right)^2 + V_{\text{eff}}(\phi, T) \right]$$

- Bubble nucleation rate per unit volume:

$$\Gamma(T) = T^4 \left(\frac{S_3}{2\pi T} \right)^{3/2} e^{-\frac{S_3}{T}}$$

Gravitational wave production

- A FOPT generates GWs from three processes: I). Bubble collisions, II). Sound wave in the plasma, III) Magnetohydrodynamic (MHD) turbulence.

- The fraction of space in the false vacuum:

$$F(t) = \exp\left[-\frac{4\pi}{3} v_w^3 \int_{t_c}^{t} dt' (t - t')^3 \Gamma(t')\right]$$

- The percolation temperature $T_\star$ of FOPT is determined by :

$$F(t_\star) = 1/e \simeq 0.37$$

Gravitational wave production

- A FOPT generates GWs from: I). Bubble collisions

$$h^2\Omega_{\rm env}(f) \;=\; 1.67\times 10^{-5}\left(\frac{H_*}{\beta}\right)^2\left(\frac{\kappa\alpha}{1+\alpha}\right)^2\left(\frac{100}{g_*}\right)^{\frac{1}{3}}\left(\frac{0.11\,v_w^3}{0.42+v_w^2}\right)S_{\rm env}(f)$$

C.Caprini et. al: 1512.06239

$$S_{\rm env}(f)=\frac{3.8\,(f/f_{\rm env})^{2.8}}{1+2.8\,(f/f_{\rm env})^{3.8}}$$

- The peak frequency is determined by the time scale of FOPT $1/\beta$:

$$\frac{f_*}{\beta}=\left(\frac{0.62}{1.8-0.1v_w+v_w^2}\right)$$

Gravitational wave production

- A FOPT generates GWs from: I). Bubble collisions

$$h^2\Omega_{\rm env}(f) \;=\; 1.67\times 10^{-5}\left(\frac{H_*}{\beta}\right)^2\left(\frac{\kappa\alpha}{1+\alpha}\right)^2\left(\frac{100}{g_*}\right)^{\frac{1}{3}}\left(\frac{0.11\,v_w^3}{0.42+v_w^2}\right)\,S_{\rm env}(f)$$

C.Caprini et. al: 1512.06239

$$S_{\rm env}(f) = \frac{3.8\,(f/f_{\rm env})^{2.8}}{1+2.8\,(f/f_{\rm env})^{3.8}}$$

- The peak frequency is determined by the time scale of FOPT. Then red-shift to present epoch

$$f_{\rm env} = 16.5\times 10^{-3}\,{\rm mHz}\left(\frac{f_*}{\beta}\right)\left(\frac{\beta}{H_*}\right)\left(\frac{T_*}{100\,{\rm GeV}}\right)\left(\frac{g_*}{100}\right)^{\frac{1}{6}}$$

Gravitational Wave

- GW spectra from the benchmark points:

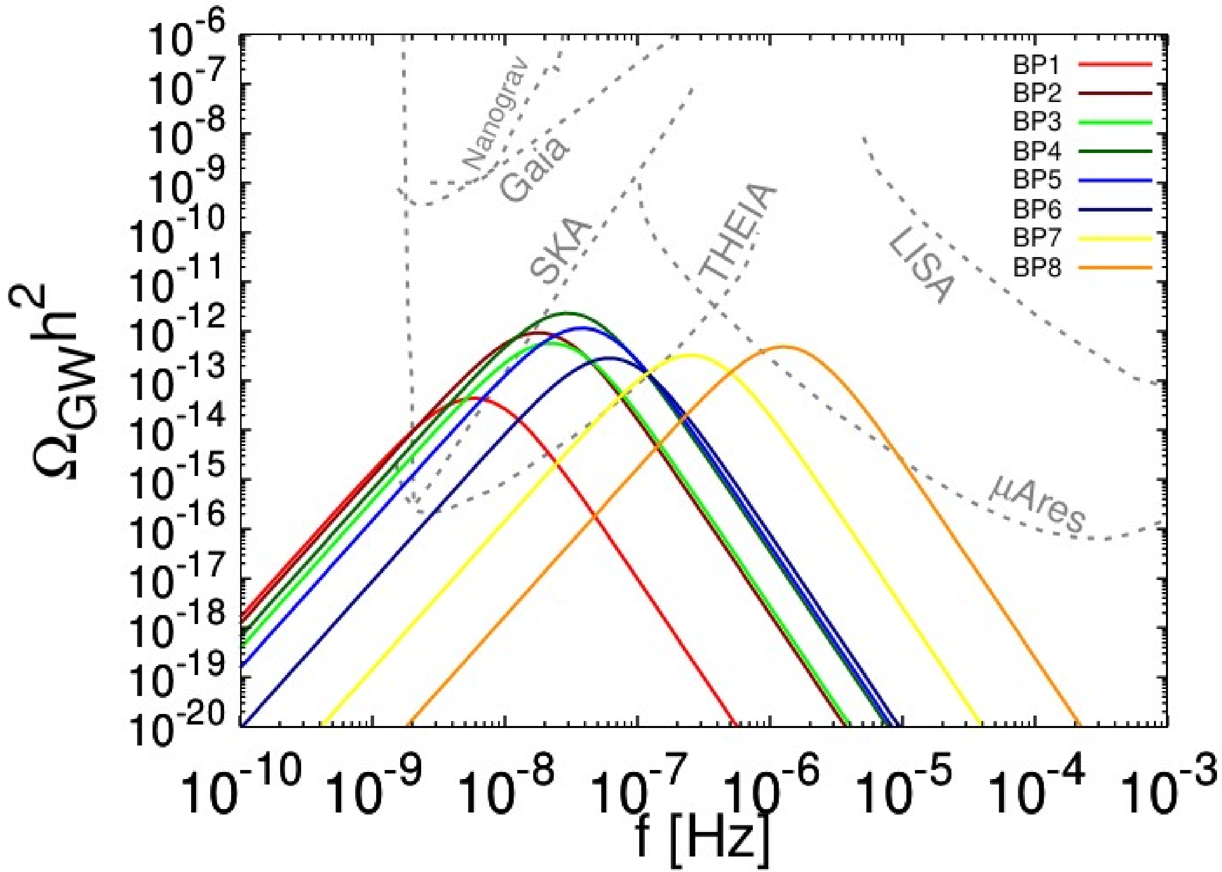

D.Marfatia, P.Y. Tseng: 2107.00859

PBH: benchmark points

- Benchmark points for PBHs from FOPT.

D.Marfatia, P.Y. Tseng:2112.14588

	BP-1	BP-2	BP-3	BP-4	BP-5	BP-6
λ	0.061	0.110	0.195	0.087	0.150	0.158
$B^{1/4}$/MeV	75.14	13.81	1.501	1.261	0.121	2.999
C/MeV	0.249	0.462	0.078	0.052	0.011	0.325
D	0.596	1.458	1.119	0.596	1.418	0.519
g_χ	1.088	1.301	1.011	1.289	0.983	1.228
η_χ	1.03×10^{-9}	1.28×10^{-10}	1.64×10^{-12}	1.21×10^{-15}	2.59×10^{-18}	6.26×10^{-17}
m/MeV	53.41	0.120	0.259	0.394	0.341	1.704
$T_{\text{SM}\star}$/MeV	94.68	14.63	0.895	2.104	0.164	4.774
$T_\star$/MeV	53.16	6.143	0.421	0.868	0.052	2.287
T_f/MeV	59.63	6.888	0.472	1.023	0.068	2.571
T_ϕ/MeV	53.09	6.045	0.415	0.857	0.050	1.950
$S_3(T_\star)/T_\star$	155	159	166	171	180	170
$M_{\text{PBH}}/M_\odot$	2.92×10^{-16}	1.15×10^{-16}	1.19×10^{-17}	1.93×10^{-18}	3.91×10^{-19}	4.23×10^{-20}
Q_{FB}	1.26×10^{42}	4.31×10^{42}	5.96×10^{42}	5.01×10^{41}	7.58×10^{41}	4.18×10^{39}
β'	2.80×10^{-17}	2.54×10^{-19}	7.78×10^{-23}	4.45×10^{-26}	5.75×10^{-30}	8.97×10^{-28}
α	1.48×10^{-2}	7.40×10^{-3}	1.20×10^{-2}	1.12×10^{-2}	1.35×10^{-2}	1.30×10^{-2}
$\beta/H_\star$	4.41×10^{3}	9.36×10^{3}	3.21×10^{4}	3.25×10^{3}	4.94×10^{3}	2.64×10^{3}
v_w	0.904	0.904	0.904	0.930	0.963	0.905
v_ϕ/MeV	224	23.1	1.426	3.821	0.247	8.157
$dM_{\text{FB}}/dQ_{\text{FB}}$/MeV	258	28.3	1.980	4.264	0.573	10.89
$\Omega_{\text{PBH}}h^2$	0.079	1.12×10^{-3}	1.09×10^{-6}	1.52×10^{-9}	2.15×10^{-13}	6.35×10^{-29}
ΔN_{eff}	0.218	0.126	0.208	0.146	0.147	0.221

FOPT->FB->PBH

- FOPT → FB → PBH.

D.Marfatia, P.Y. Tseng:2112.14588

- During the FB formation, the Yukawa potential must not dominate the FB energy:

$$T_\star > T_\phi$$

- FB is stable:

$$\frac{dM_{\rm FB}}{dQ_{\rm FB}} < m + g_\chi v_\phi, \quad \text{and} \quad \frac{d^2 M_{\rm FB}}{dQ_{\rm FB}^2} < 0$$

FOPT->FB->PBH

D.Marfatia, P.Y. Tseng:2112.14588

- FOPT → FB → PBH.
- During the FB formation, the Yukawa potential must not dominate the FB energy:

$$T_\star > T_\phi$$

- FB is stable:

Green: GW
Red: GW+gamma-ray
Yellow: gamma-ray

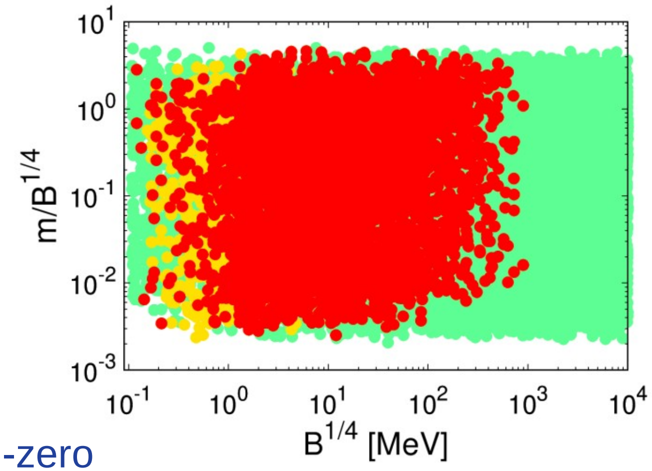

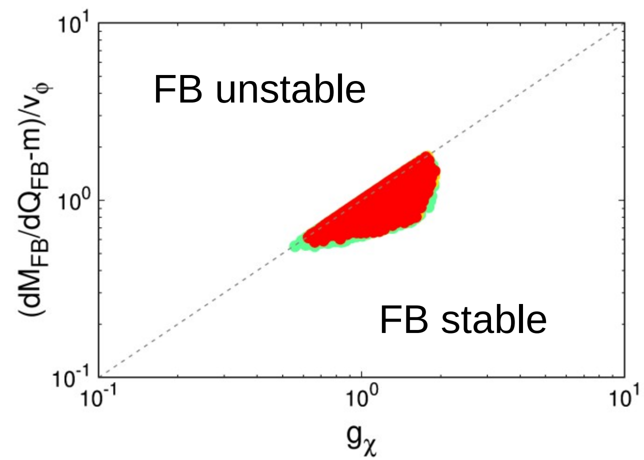

DM bare mass is non-zero

Gravitational Wave

- GW spectra from the benchmark points:

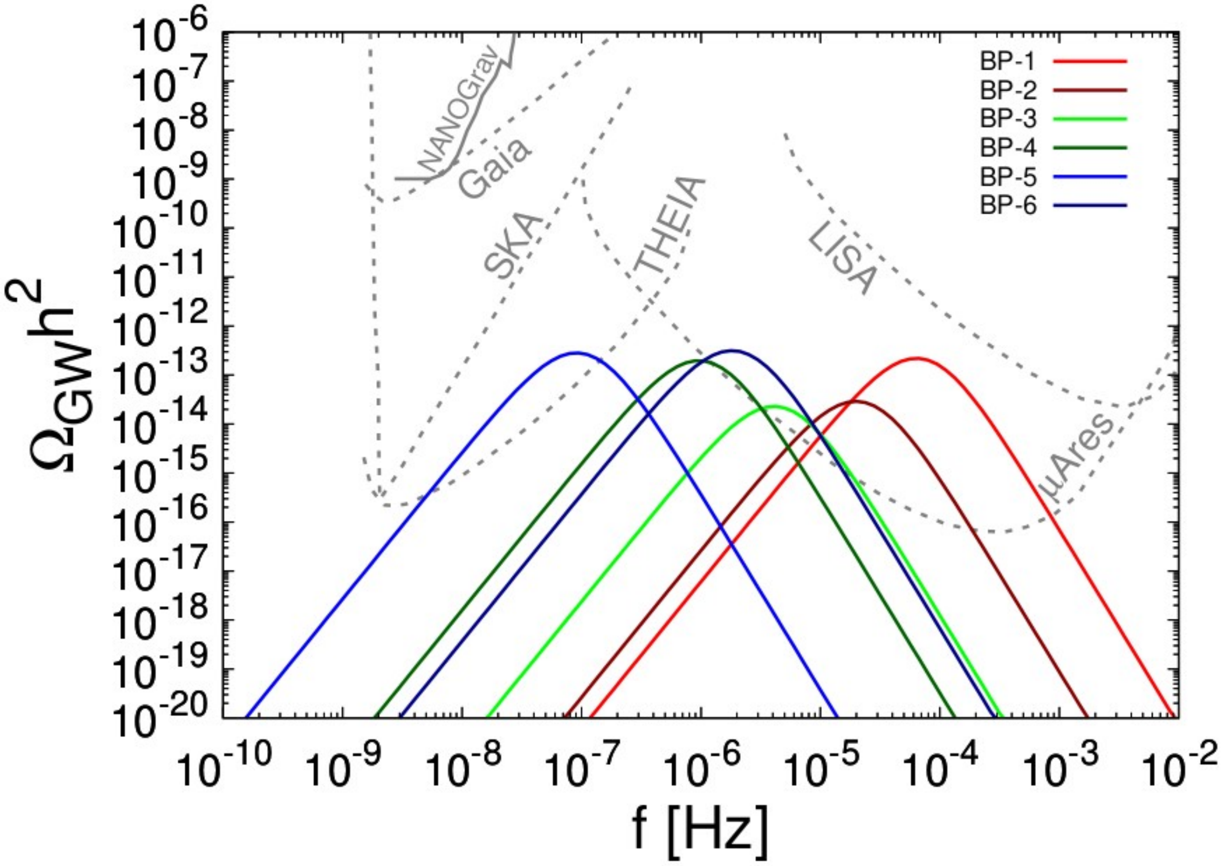

D.Marfatia, P.Y. Tseng: 2112.14588

PBH evaporation

- The evaporation of a PBH produces all particles with mass below the PBH temperature: Kazunori Kohri et.al: 2002.12778

$$T_{\rm PBH} \simeq 5.3\ {\rm MeV} \times \left(\frac{10^{-18} M_\odot}{M_{\rm PBH}}\right)$$

- For $M_{\rm PBH}/M_\odot \lesssim 2 \times 10^{-19}$, PBHs evaporated before today.

- The Hawking emission rate of primary particles:

$$\frac{dN_i}{dEdt} = \frac{n_i^{\rm d.o.f}\Gamma_i(E, M_{\rm PBH})}{2\pi(e^{E/T_{\rm PBH}} \pm 1)}$$

A.Arbey, J.Auffinger (BlackHawk): 1905.04268

PBH evaporation

- The extragalactic gamma-ray background due to PBH evaporation

Kazunori Kohri et.al: 2002.12778

$$\frac{d^2\Phi}{dEdt} = \int_{t_{\rm CMB}}^{\min(t_{\rm eva},t_0)} c[1+z(t)]\frac{f_{\rm PBH}\rho_{\rm DM}}{M_{\rm PBH}}\frac{d^2N_\gamma}{d\tilde{E}dt}\bigg|_{\tilde{E}=[1+z(t)]E} dt$$

with average DM density $\rho_{\rm DM} = 1.27\ {\rm GeV\,m^{-3}}$.

- The evolution of the Universe is approximated as matter dominated until the current epoch

$$1+z(t) = \left(\frac{t_0}{t}\right)^{2/3}$$

Correlated GW and gamma-ray signals

- β' is defined at PBH formation as:

Kazunori Kohri et.al: 2002.12778

$$\beta' \equiv \gamma^{1/2} \left(\frac{g_*(T_\phi)}{106.75} \right)^{-1/4} \left(\frac{h}{0.67} \right)^{-2} \frac{\rho_{\rm PBH}(T_\phi)}{\rho(T_\phi)}$$

- γ is the ratio between BH mass to the horizon mass in radiation dominated era. In our scenario, it gives

$$\gamma^{1/2} \left(\frac{g_*(T_\phi)}{106.75} \right)^{-1/4} = 4.58 \times 10^{-12} \frac{T_\phi}{\rm MeV} \left(\frac{M_{\rm PBH}}{10^{-18} M_\odot} \right)^{1/2}$$

Correlated GW and gamma-ray signals

- Correlated signals of GW and extragalactic gamma-ray:

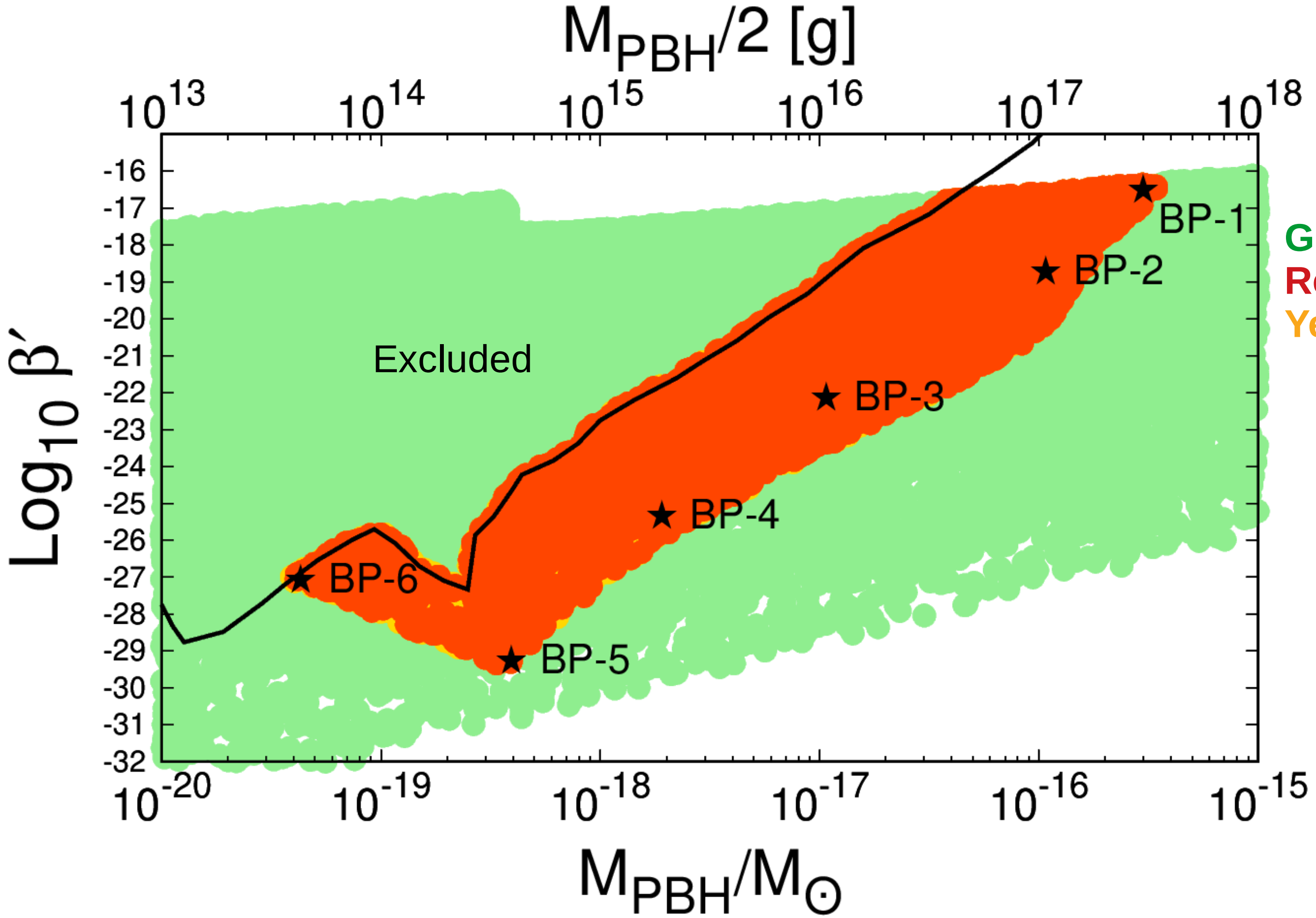

Green: GW
Red: GW+gamma-ray
Yellow: gamma-ray

Gamma-ray signal

- The extragalactic gamma-ray background due to PBH evaporation for the benchmark points

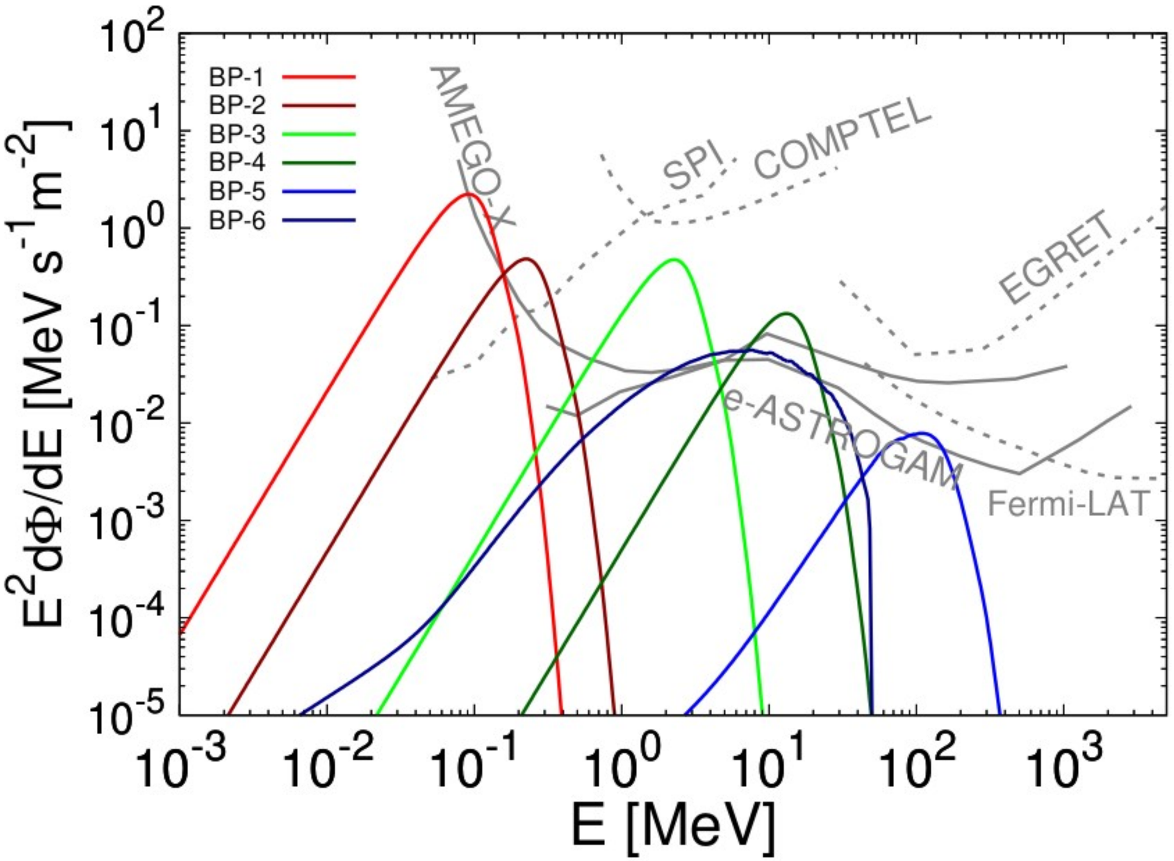

Part-1: Bubble wall velocity

- Particles reflected by the bubble wall exert pressure on it, and slow down the bubble wall velocity.

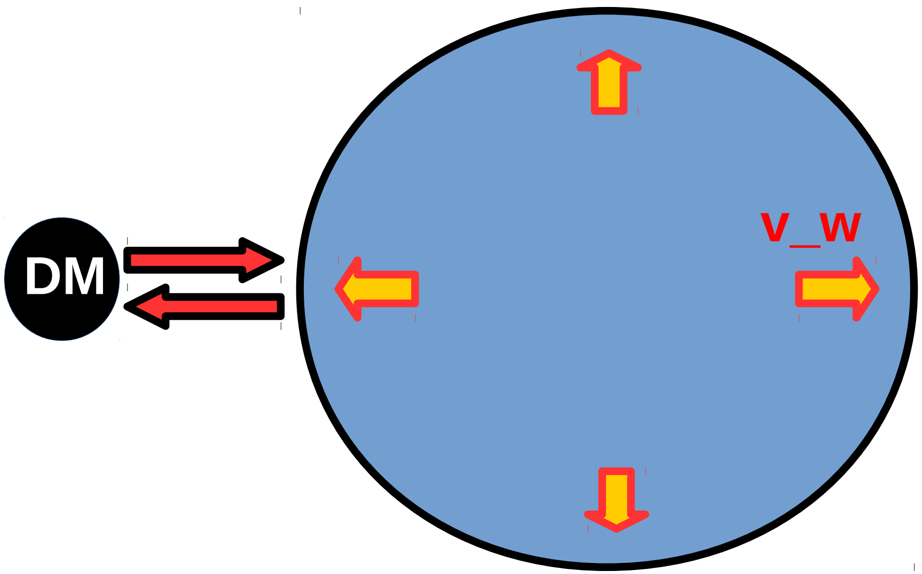

Part-1: Bubble filtering

- If a thermal DM flux is incident on the wall, the number density of DM that enter the bubble is:

$$n_\chi^{\rm in} = n_{\bar\chi}^{\rm in} \simeq \frac{g_{\rm DM} T_\star^3}{\gamma_w v_w} \left(\frac{\gamma_w (1-v_w) m_\chi / T_\star + 1}{4\pi^2 \gamma_\omega^3 (1-v_w)^2} \right) e^{-\frac{\gamma_w (1-v_w) m_\chi}{T_\star}}$$

D.Chway, T.H.Jung, C.S.Shin: 1912.04238

- DMs are filtered by the non-relativistic and relativistic bubble wall velocity:

$$n_\chi^{\rm in} = \begin{cases} \sim e^{-m_\chi/T_\star} & \text{for} \quad v_w \to 0 \\ \sim e^{-m_\chi/(2\gamma_w T_\star)} & \text{for} \quad m_\chi/(\gamma_w T_\star) \to 0 \end{cases}$$

Part-1: Bubble filtering

- If $T_\star < T_{\rm dec}$, the DM inside the bubble is decoupled from the thermal bath and become DM relic abundance.

- DM relic abundance today can be calculated by dividing $n_\chi^{\rm in}+n_{\bar\chi}^{\rm in}$ by entropy $s = (2\pi^2/45)g_{\star S}T^3$:

$$\Omega_{\rm DM}h^2 \simeq 6.29 \times 10^8 \, \frac{m_\chi (n_\chi^{\rm in} + n_{\bar\chi}^{\rm in})}{\rm GeV} \frac{1}{g_{\star S} T_\star^3}$$

$$\Omega_{\rm DM}h^2 \simeq \begin{cases} 1.27 \times 10^8 \left(\frac{m_\chi}{\rm GeV}\right)\left(\frac{g_{\rm DM}}{g_{\star S}}\right)\left(\frac{m_\chi}{2\gamma_w T_\star}+1\right) e^{-\frac{m_\chi}{2\gamma_w T_\star}}\,, & \text{for } v_w \to 1 \\ 3.19 \times 10^7 \left(\frac{m_\chi}{\rm GeV}\right)\left(\frac{g_{\rm DM}}{g_{\star S}}\right)\left(\frac{1}{v_w}\right)\left(\frac{m_\chi}{T_\star}+1\right) e^{-\frac{m_\chi}{T_\star}}\,, & \text{for } v_w \to 0. \end{cases}$$

Part-1: Bubble filtering

- If $T_\star < T_{\rm dec}$, the DM inside the bubble is decoupled from the thermal bath and become DM relic abundance.
- DM relic abundance today can be calculated by dividing $n_\chi^{\rm in} + n_{\bar{\chi}}^{\rm in}$ by entropy $s = (2\pi^2/45) g_{\star S} T^3$:
- For example: $m_\chi \simeq 1 \text{ TeV}, \, v_w \to 1$ requires

$$\boxed{\frac{m_\chi}{2\gamma_w T_\star} \simeq 27}$$

Part-1: Bubble filtering

- If $T_\star < T_{\rm dec}$, the DM inside the bubble is decoupled from the thermal bath and become DM relic abundance.

- DM relic abundance today can be calculated by dividing $n_\chi^{\rm in} + n_{\bar\chi}^{\rm in}$ by entropy $s = (2\pi^2/45) g_{\star S} T^3$:

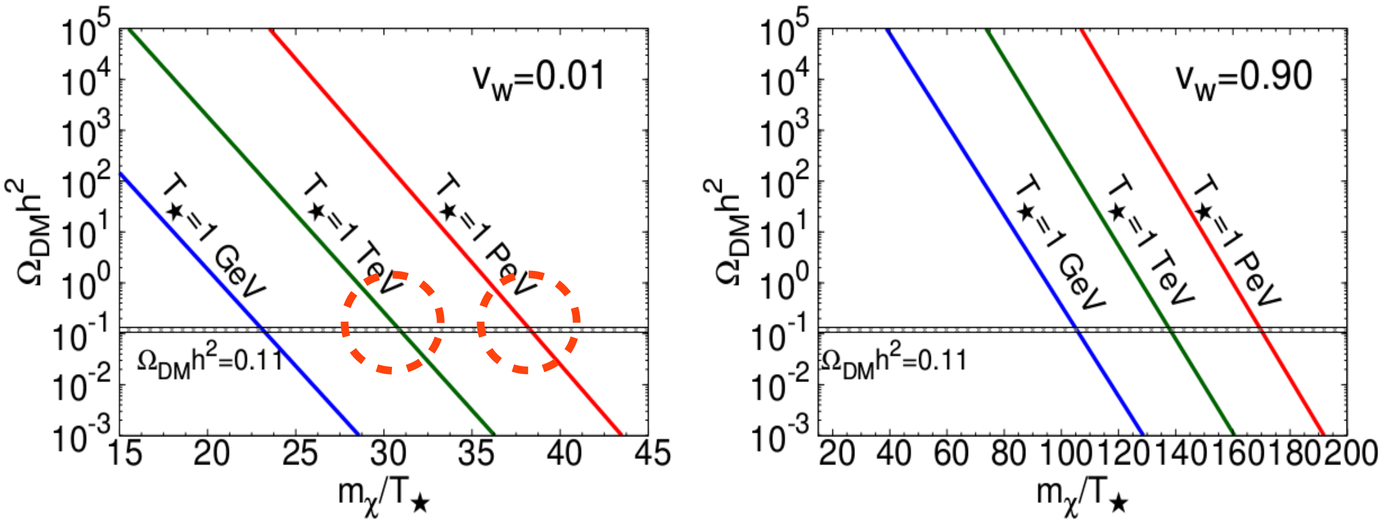

Part-1: Bubble filtering

- Sudden DM freeze-out induced by a FOPT can easily accommodate DM mass above a PeV, which is beyond the current DM direct detection and LHC searches.

- We focus on the Gravitational Wave (GW) signals of Sudden DM freeze-out with a FOPT.

Part-1: Scalar quartic Model

- The finite-temperature quartic effective scalar potential is:

$$V_{\text{eff}}(\eta, T) = \frac{\mu^2 + DT^2}{2}\eta^2 - \xi T \eta^3 + \frac{\lambda}{4}\eta^4$$

F.C.Adams: hep-ph/9302321

- Including one-loop Coleman-Weinberg and finite-temperature contributions, potentials of this form are commonly found in *inert singlet*, *inert doublet*, *MSSM*, *and Majoron models*.

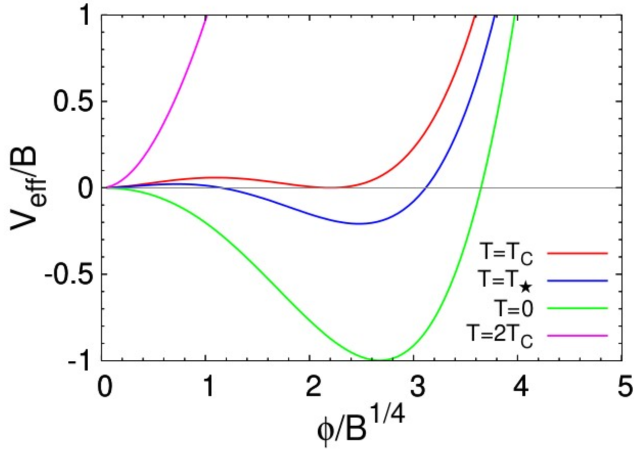

Part-1: Scalar quartic Model

- The finite-temperature quartic effective scalar potential is:

$$V_{\rm eff}(\eta, T) = \frac{\mu^2 + DT^2}{2}\eta^2 - \xi T\eta^3 + \frac{\lambda}{4}\eta^4$$

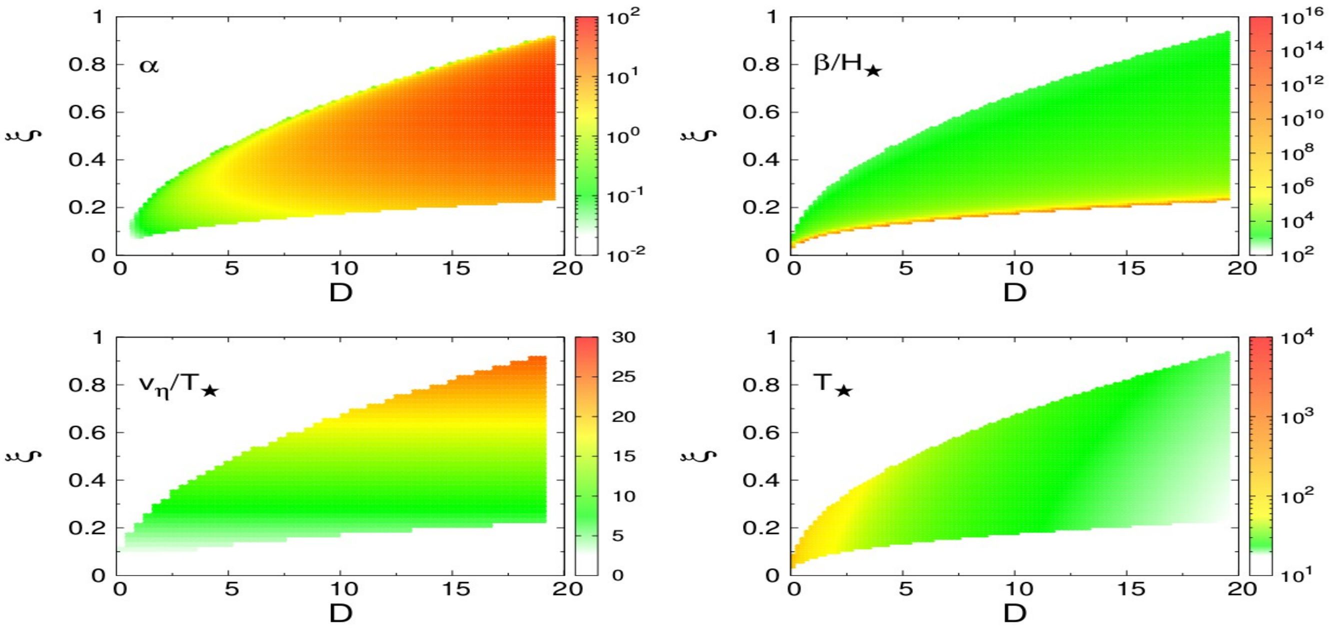

Figure 2. The parameters α, β/H, $v_\eta/T_\star$, and $T_\star$ for the Scalar Quartic Model with $\lambda = 0.1$.

D.Marfatia, P.Y. Tseng: 2006.07313

Part-1: Scalar quartic Model

- The finite-temperature quartic effective scalar potential is:

$$V_{\rm eff}(\eta, T) = \frac{\mu^2 + DT^2}{2}\eta^2 - \xi T\eta^3 + \frac{\lambda}{4}\eta^4$$

- Correct DM relic:

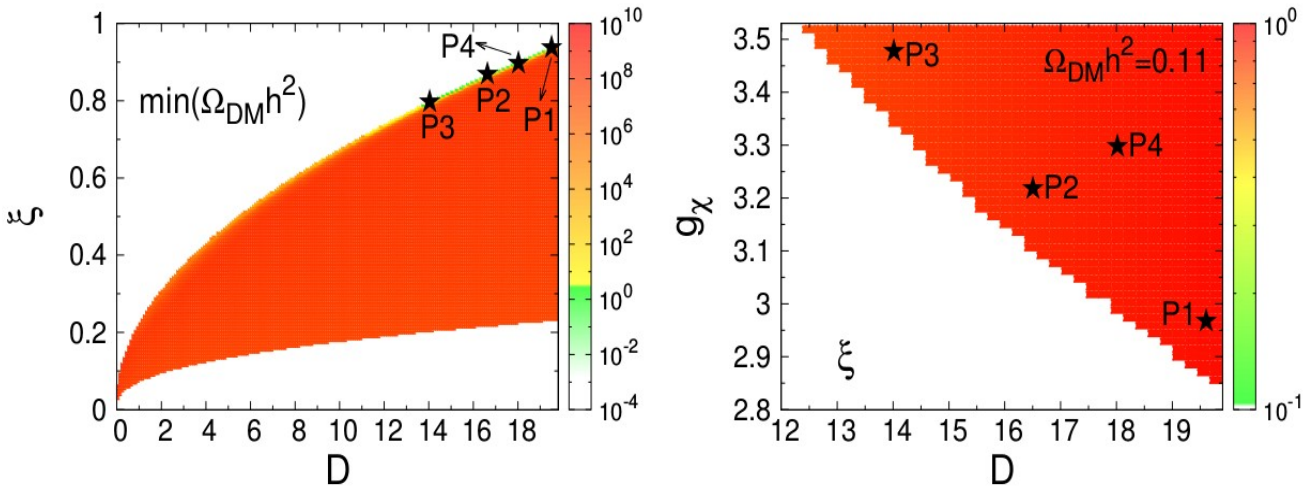

D.Marfatia, P.Y. Tseng: 2006.07313

Part-1: Scalar quartic Model

- The finite-temperature quartic effective scalar potential is:

$$V_{\text{eff}}(\eta, T) = \frac{\mu^2 + DT^2}{2}\eta^2 - \xi T\eta^3 + \frac{\lambda}{4}\eta^4$$

- Benchmark points:

Table 1. Benchmark points (with $\lambda = 0.1$) for the Scalar Quartic Model that give $\Omega_{\text{DM}}h^2 = 0.11$.

	P1	**P2**	**P3**	**P4**
ξ	0.943	0.863	0.796	0.901
D	19.7	16.5	14.0	18.0
g_χ	2.97	3.22	3.48	3.31
α	0.089	0.082	0.076	0.121
$\beta/H_\star$	1116	1062	1015	1085
$v_\eta/T_\star$	25.71	23.41	21.49	24.51
v_w	0.768	0.763	0.760	0.791
$T_\star$/GeV	21.5	23.8	26.1	22.7
m_χ/GeV	1642	1799	1953	1838

D.Marfatia, P.Y. Tseng: 2006.07313

Part-1: Scalar quartic Model

- The finite-temperature quartic effective scalar potential is:

$$V_{\rm eff}(\eta, T) = \frac{\mu^2 + DT^2}{2}\eta^2 - \xi T\eta^3 + \frac{\lambda}{4}\eta^4$$

- GW signals:

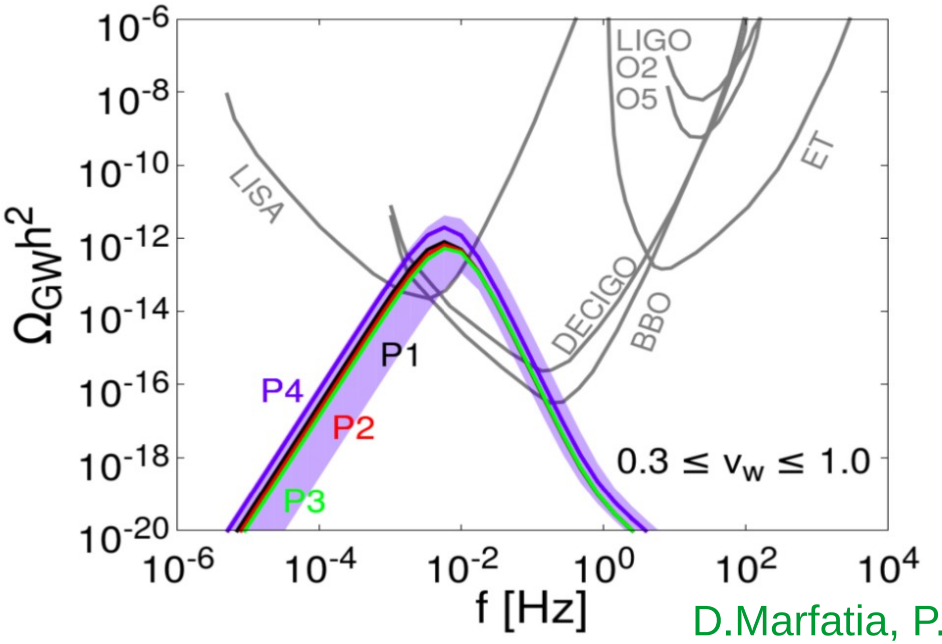

D.Marfatia, P.Y. Tseng: 2006.07313

Part-1: Summary

- We studied the sudden freeze-out DM as an alternative to the continuous thermal freeze-out.
- A necessary ingredient is a FOPT generates DM mass.
- The DM relic abundance may be determined by bubble filtering.
- Because FOPT triggers sudden DM freeze-out, GW offers a signature.

Part-1: Introduction

- The $m_\chi/T_\star$ needed to produce the DM relic abundance depends on the velocity of bubble wall v_w .

$$T_\star = m_\chi/30 \text{ for } m_\chi = 1 \text{ TeV}, v_w = 0.01$$

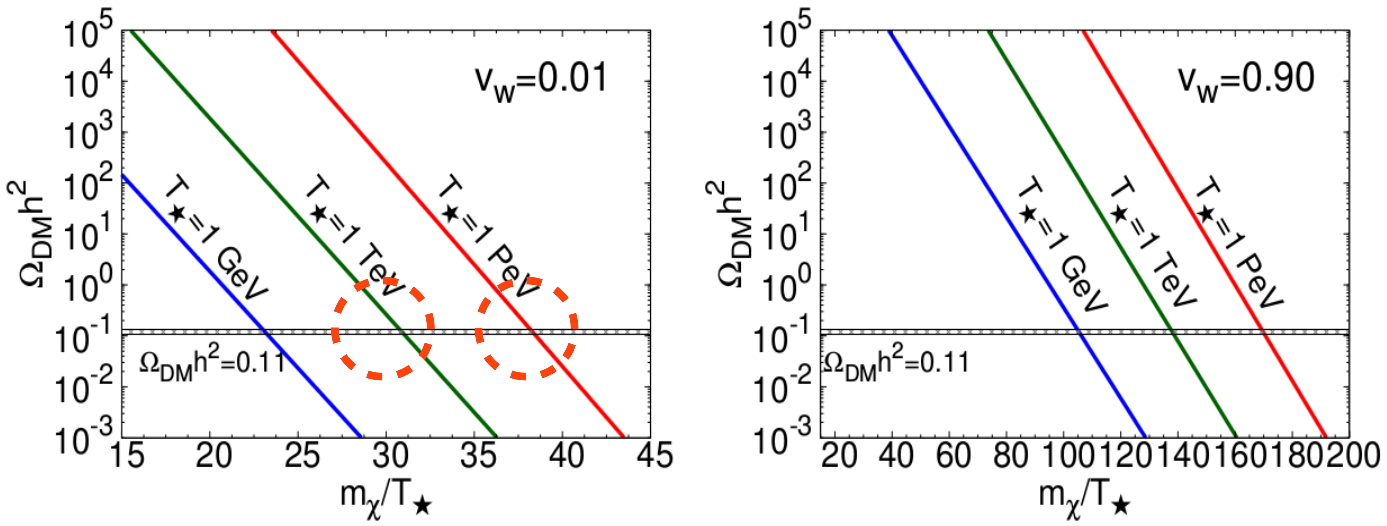

Part-1: Bubble wall velocity

- In the ultrarelativistic limit, the pressure on bubble wall can be obtain from the light degree of freedom inside and outside the bubble:

D.Chway et.al : 1912.04238
J.R.Espinosa et.al: 1004.4187
D.Bodeker et.al : 0903.4099

$$P = \frac{d_n g_\star \pi^2}{90}(1+v_w)^3\gamma_\omega^2 T_\star^4$$

$$d_n \equiv \frac{1}{g_\star}\left[\sum_{0.2M_i>\gamma_w T_\star}\left(g_i^b + \frac{7}{8}g_i^f\right)\right]$$

- The v_w can be obtained by solving the eq. $P = \Delta V_{\rm eff}$:

$$\alpha = \frac{d_n}{3}(1+v_w)^3\gamma_\omega^2$$

$$\alpha \equiv \frac{\left(1-T\frac{\partial}{\partial T}\right)\Delta V_{\rm eff}|_{T_\star}}{\rho(T_\star)}, \quad \rho \equiv \pi^2 g_\star T^4/30$$

Part-1: Bubble wall velocity

- For bubble wall velocity v_w faster than the sound speed in plasma, but not ultrarelativistic, we use the approximation:

P.J.Steinhardt, Phys. Rev. D. 25, 2074 (1982)

$$v_w = \frac{\frac{1}{\sqrt{3}} + \sqrt{\alpha^2 + \frac{2}{3}\alpha}}{1+\alpha}$$

Part-2: anti-correlation

- The percolation condition using saddle point approximation:

$$F(t) = \exp\left[-\frac{4\pi}{3} v_w^3 \int_{t_c}^{t} dt' (t-t')^3 \Gamma(t')\right]$$

$$F(t_\star) = 1/e \simeq 0.37$$

$$8\pi v_w^3 \Gamma(T_\star) \beta^{-4} \simeq 1$$

- Since $\beta/H_\star$ is almost constant, thus $\beta \propto H_\star \propto T_\star^2$ and from above condition, we have

$$T_\star^{-4}\, e^{-S_3(T_\star)/T_\star} \simeq B^{-1}\, e^{-S_3(T_\star)/T_\star} \simeq \text{constant}\,, \quad \text{i.e.,} \quad e^{-S_3(T_\star)/T_\star} \propto B$$

- Bubble nucleation rate per unit volume grow with vacuum energy density.

- For fixed $\Omega_{\rm FB} h^2$, we obtain $M_{\rm FB} \propto 1/n_{\rm FB}|_{T_0} \propto e^{3/4 \cdot (S_3(T_\star)/T_\star)} \propto B^{-3/4}$

Part-2: Anti-correlation

- We consider the finite-temperature quartic effective potential.
- Anti-correlation between the FB mass and energy scale of FOPT.

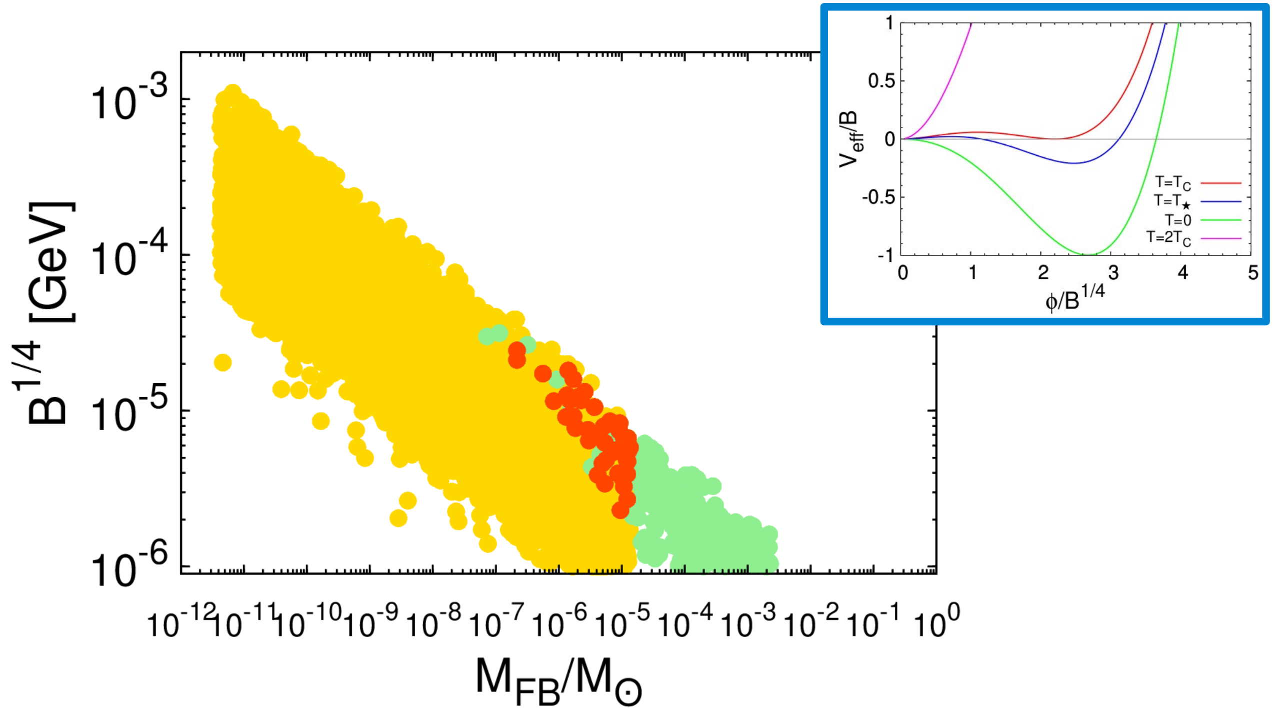

Part-2: Number density of FB

- Solving the Tolman-Oppenheimer-Volkoff(TOV) equation to find the density profile of FB

D.Marfatia, P.Y. Tseng: 2107.00859

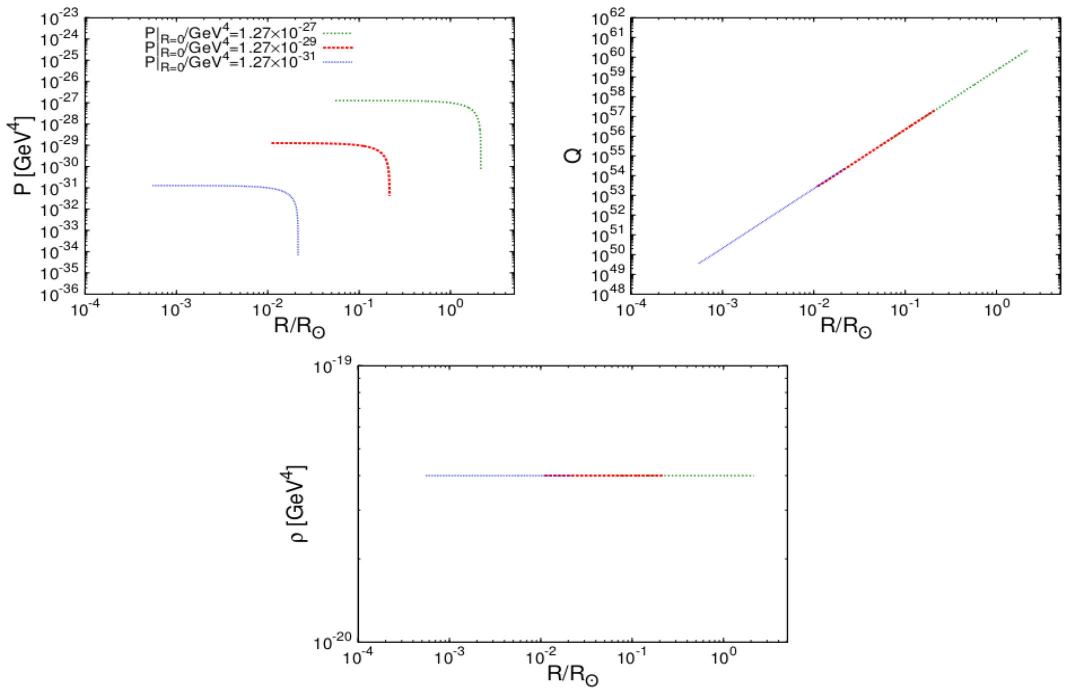

Figure 2. The pressure P (upper-left), Q-charge within radius R (upper-right), and energy density profile (bottom) of a FB with $B^{1/4} = 10$ keV for three boundary conditions, $P|_{R=0} = 1.27\times10^{-27}$ GeV^4, $P|_{R=0} = 1.27\times10^{-29}$ GeV^4, and $P|_{R=0} = 1.27\times10^{-31}$ GeV^4. Correspondingly, $(M_{\rm FB}/M_\odot, R_{\rm FB}/R_\odot) = (6.5079\times10^{-2}, 2.149)$, $(6.4911\times10^{-5}, 0.2149)$, and $(6.5079\times10^{-8}, 2.149\times10^{-2})$.

Relativistic degree of freedom

- The temperature of FOPT is lower than the BBN, and robust 95% CL upper limit is $\Delta N_{\rm eff} \lesssim 0.5$. 2009.09754:1103.1261
- We consider decoupled dark and SM sectors with temperature ratio $r_T = \frac{T_i^{\rm (D)}}{T^{\rm (SM)}}$.
- The extra effective neutrino number

Y.Nakai,M.Suzuki,F.Takahashi, M.Yamada: 2009.09754

$$\Delta N_{\rm eff} \simeq 0.49 \times \left(\frac{R}{0.13}\right)^{4/3} \left(\frac{g_{*0}^{\rm (D)}}{g_{*0}}\right) \left(\frac{g_{*s0}}{g_{*s0}^{\rm (D)}}\right)^{4/3}$$

$$g_\star^{(D)} = 2 * 2 * (7/8) + 1 = 4.5$$

- R is the entropy ratio after the phase transition.

Part-2: Correlated signals

- Correlated signals of GW and microlensing:

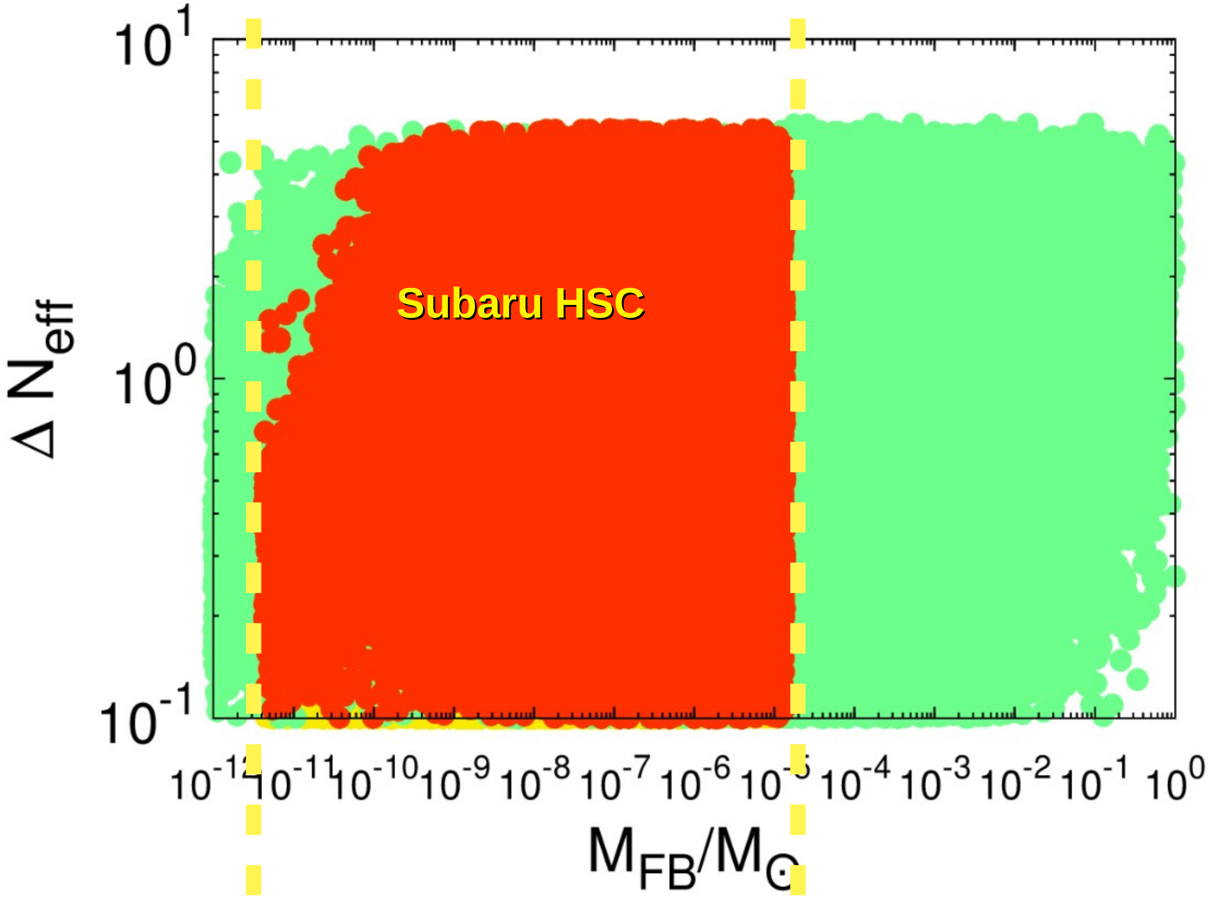

Part-2: Correlated signals

- From BBN, the robust 95% CL upper limit is $\Delta N_{\rm eff} \lesssim 0.5$.